UNIVERSITÀ DEGLI STUDI DI PADOVA

Dipartimento di Fisica e Astronomia "Galileo Galilei"

Master Degree in Astrophysics and Cosmology

Final Dissertation

Eccentricity evolution of binary black holes in globular clusters

Thesis Supervisor

Prof. Michela Mapelli

Candidate

Francesco Flora

Thesis Co-Supervisor

Prof. Mark Gieles

Dott. Marco Dall'Amico

Dott. Stefano Torniamenti

Academic Year 2021/2022

Contents

Chapter 1

Introduction

A large fraction of stars in the field are likely members of binary or multiple systems. These binaries play a notable role in the dynamics of star clusters, such as globular clusters [15]. The presence of a companion alters the evolutionary path of a star, leading to phenomena such a stellar mergers, X-ray binaries and gamma-ray bursts. However the scarcity of direct measurements of the intrinsic distributions of orbital parameters means that many details of these processes remain uncertain [39]. Moreover, the new era of gravitational wave astronomy initiated by the detection of gravitational waves from a binary black hole (BBH) by the LIGO interferometers [1] contributed to a growth in interest towards binary systems.

Star clusters, such as globular clusters, likely host the formation of the vast majority of massive stars believed to be black hole progenitors [26]. Understanding the properties of binary systems in star clusters is therefore important, but difficult from an observational point of view. Studies on the binary population of globular clusters, such as [32], focus on determining the fraction of binaries in the cluster, while extracting the orbital parameters of these systems is hard due to the large distance and high densities of globular clusters. The extraction of orbital parameters for binary systems is possible for closer star clusters such as open clusters, like in Sana et al. 2012 [39]. Analyzing the population of O-stars in six nearby galactic

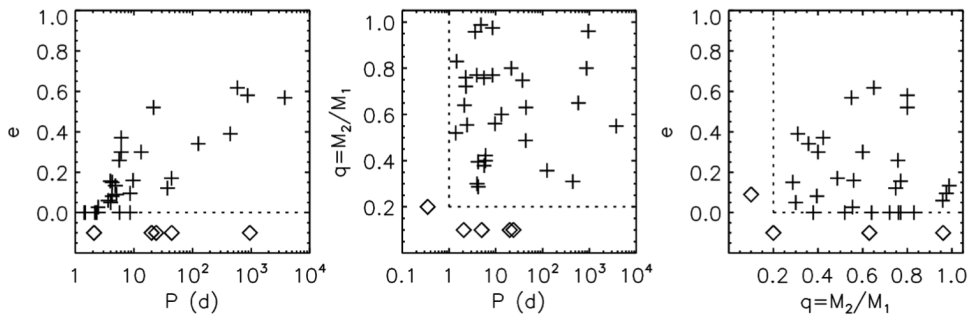

Figure 1.1: Position of binaries in the period (P) - mass-ratio (q) - eccentricity (e) plane from the sample of O stars binaries in open clusters from Sana et al. [39].

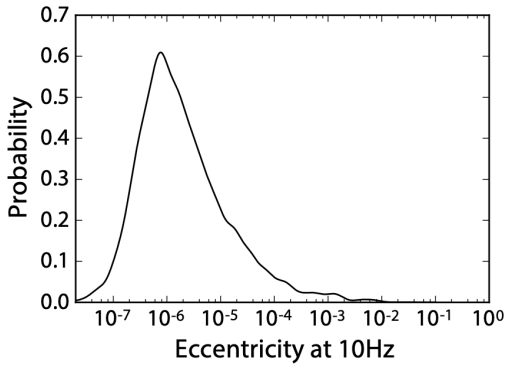

Figure 1.2: Eccentricity distribution of sources entering the LIGO frequency band [37].

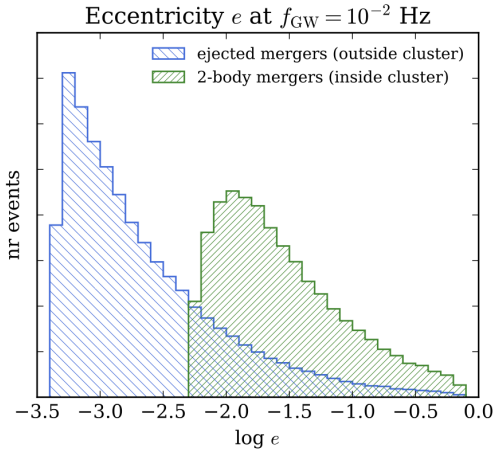

Figure 1.3: Distribution of BBH orbital eccentricity e at 10^{-2}Hz for BBHs merging inside a globular cluster or ejected from it [38].

open clusters they were able to extract the orbital parameters of roughly 30 binaries, as seen in fig. 1.1.

In this thesis work, I focused on one particular orbital parameter, the eccentricity, of a particular class of binaries called hard binaries. In a star cluster environment, like that of a globular cluster, due to their high density, binary systems are likely to interact with single stars in scattering processes. The global eccentricity distribution for binary systems in star clusters has already been extensively studied ([24],[16],[25],[11]); it is called *thermal distribution* and takes the following form: $f(e) = 2\,e$. However this applies to a cluster as a whole, under the assumption of thermal equilibrium. The goal of this thesis is to show that scattering events tend to increase the eccentricity of hard binaries, and I obtained this result by modelling individual binary-single encounters with the high precision N-body code ARWV [7].

The eccentricity is also a relevant parameter for what concerns gravitational-wave signals from BBH mergers. At the frequencies at which ground based detector operate ($10 - 10^4$ Hz), as a consequence of the circularization of the orbits due to gravitational wave emission [33], 99% of sources enter the LIGO band with

eccentricities below $\sim 10^{-3}$ [37] (see fig. 1.2). However future space-borne detectors like LISA [2], operating at much lower frequencies (10^{-2}Hz), will be able to detect BBHs mergers with measurable eccentricities $e > 0.01$ [38], as seen in fig. 1.3

In chapter 2 I will provide an overview of what a globular cluster is, and I will describe a collection of models to describe them. I will also describe some key processes that play an important role in the star cluster evolution. In chapter 3, I will describe the dynamics of binary systems, focusing in particular on the description of three-body encounters. I will also discuss the thermal eccentricity distribution as the global distribution of binary eccentricities. In chapter 4, I will describe the code ARWV and why it is suitable for the investigation performed in this work. I will also carefully describe the initial conditions for our scattering experiments and discuss the outcomes of such experiments. Finally in chapter 5 I will illustrate a code I developed, based on a Monte Carlo approach, that aims at modelling the energy and eccentricity evolution of binary systems as a consequence of scattering events. I used this code to demonstrate a result obtained in the previous chapter, but with a different, analytic approach. The result in question is that a particular type of encounter, called *flyby*, contributes less to the eccentricity evolution compared to another class of encounters called *exchanges*.

Chapter 2

Globular Clusters

Globular clusters are large, dense, self-gravitating, almost collisionless agglomerates of stars. They are characterized by a half-light radius with typical values of $3-5\,\mathrm{pc}$, up to a few tens of pc, central mass density $\rho_c \geq 10^4\,\mathrm{M}_\odot\mathrm{pc}^{-3}$, and ages of around $10\,\mathrm{Gyr}$ up to $\sim 12\,\mathrm{Gyr}$ [15, 26]. They are normally associated with a host galaxy, and most galaxies, like the Milky Way, host several of these systems [4] (see fig. 2.2).

2.1 Evolution of a globular cluster

Globular clusters (and star clusters in general), are *collisional systems*. In a collisional system the relaxation timescale t_r (the time needed for a star in the cluster to loose memory of its initial velocity as a consequence of two-body interactions) is smaller than the lifespan of the cluster. The two-body relaxation timescale is the time needed for a star in the cluster to loose memory of its initial velocity as a consequence of two-body encounters. The two-body relaxation timescale is defined as [26, 42]:

$$t_\mathrm{r} = 0.34\frac{\sigma^3}{G^2\langle m\rangle\rho\ln(0.4N)}, \tag{2.1}$$

where σ is the velocity dispersion of the stars in the star cluster, $\langle m\rangle$ is the average mass of the stars, ρ is the local mass density and N is the number of stars in the cluster. This expression is valid if the only interaction considered is the gravitational pull between stars, and the gravitational potential of the cluster is assumed to be spherically symmetric. For globular clusters the two-body relaxation timescale is smaller than the lifespan of the star cluster, with a value of $t_\mathrm{r} \sim 10^9 yr$ [36]. Fig. 2.3 shows a radius-mass diagram for star clusters in the Milky Way, and relaxation times are also highlighted. In such a system the interactions between stars are common, and produce a *granularity* of the gravitational field [43]. The gravitational field will be constantly fluctuating, resulting in local changes of the magnitude and directions of star velocities. This random reshuffling of the velocities will reduce deviations from the equilibrium distribution for the velocities, i.e. a Maxwellian distribution [10]. This facilitates the *evaporation* of the cluster, an important process for the

Figure 2.1: Hubble Space Telescope photograph of the dense globular cluster M80 (NGC 6093) [4].

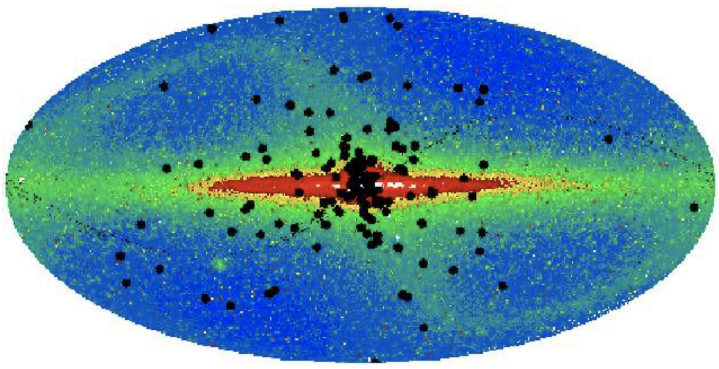

Figure 2.2: Globular clusters positions about the Milky Way superimposed to a map of the galaxy from the COBE satellite using a Mollweide projection [4].

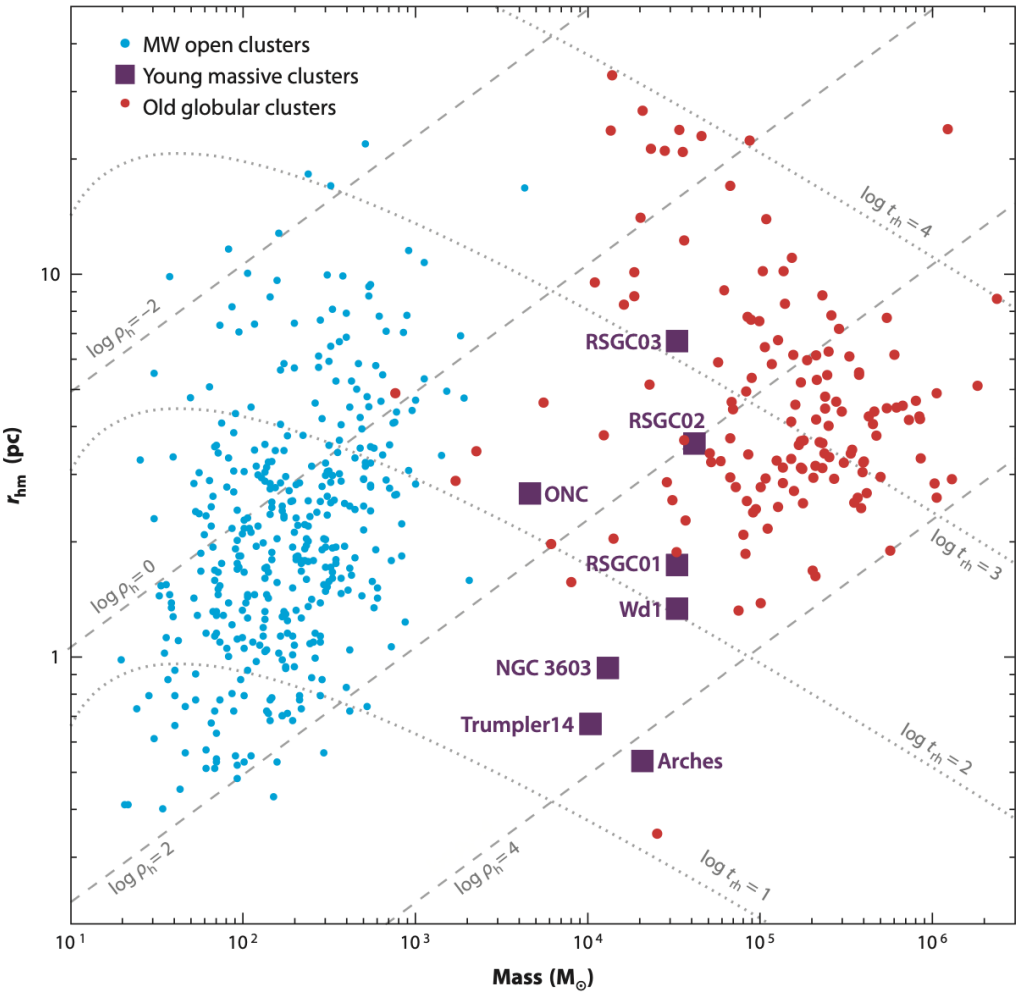

Figure 2.3: Radius-mass diagram for open clusters, young massive clusters and old globular clusters in the Milky Way. Relaxation times in Myr are also highlighted [36].

evolution of the cluster. Another process relevant for the evolution of the cluster is the *core collapse*, also called *gravothermal catastrophe*, related as well to the evaporation process and therefore to the granularity of the gravitational potential.

2.1.1 Zero-order models

Ignoring for a moment the granularity of the gravitational field we can briefly discuss, following Spitzer 1987 [42], some simple models to describe a globular cluster. These idealized models ignore stellar encounters and other effects to allow for steady-state solutions and equilibrium configurations. The gravitational potential will then be a slowly varying function of the position. We can define a velocity distribution function $f(\mathbf{x}, \mathbf{v}, t)$, defined so that the quantity $f(\mathbf{x}, \mathbf{v}, t)\, d^3\mathbf{x} d^3\mathbf{v}$ is the number of particles in the volume $d^3\mathbf{x}$ with velocities in $d^3\mathbf{v}$. This distribution function satisfies the collisionless Boltzmann equation:

$$\frac{\partial f}{\partial t} + \mathbf{v} \cdot \frac{\partial f}{\partial \mathbf{x}} + \mathbf{a} \cdot \frac{\partial f}{\partial \mathbf{v}} = 0, \tag{2.2}$$

which can be derived from the conservation of particles, and where $a_i = dv_i/dt$. The acceleration is related to the gravitational potential ϕ as:

$$a_i = -\frac{\partial \phi}{\partial x_i}, \tag{2.3}$$

and coupling eq. (2.2) with the Poisson equation for the gravitational potential:

$$\nabla^2 \phi(\mathbf{x}, t) = 4\pi G \rho, \tag{2.4}$$

it is possible to describe the dynamical evolution of the system [20].

For the purpose of describing the zero-order models we can introduce two further assumptions, in order to consider systems with spherical symmetry in steady-state equilibrium:

- The gravitational potential ϕ, the distribution function f and the other quantities describing the cluster's properties are independent of time.

- We impose the spherical symmetry: ϕ depends only on the radial coordinate r, and f depends only on r, v_r, v_t, where v_t is the velocity transverse to the radial direction.

With these assumptions we can discuss some zero-order models:

1. The simplest model is a sphere where the motion of stars simply balances the the gravitational pull:
$$v_r = 0, \quad v_t = \frac{GM(r)}{r}. \tag{2.5}$$

2. If we assume an isotropic velocity distribution, with:

$$\begin{cases} f = \kappa_1(-E)^p & \text{for } E > 0 \\ 0 & \text{for } E < 0, \end{cases} \tag{2.6}$$

where $E = E = \frac{1}{2}v^2 + \phi(r)$, κ_1 is a constant and $\phi(r)$ is equal to zero outside the cluster surface, we obtain the following function for the density of the cluster:

$$\rho(r) = \kappa_2[-\phi(r)]^n, \tag{2.7}$$

where $n = p + 3/2$ and κ_2 is a constant. Analytic solutions can be found for $n = 0$ (*uniform sphere* with constant density), $n = 1$, $n = 5$. This last case is particularly interesting since it was used by Plummer to fit observations of globular clusters [34]. It is therefore called *Plummer model* [4], and describes a cluster with a compact core, and extended outer envelope. Even though this cluster does not have external boundaries, it contains a finite number of stars.

3. The next class of models we mention is that of the *isothermal spheres*. In these models the velocity distribution function f approaches a value f^0 in statistical equilibrium:

$$f^0 = \kappa \exp^{-3E/\langle v^2 \rangle}, \tag{2.8}$$

where $\langle v^2 \rangle$ is the mean square velocity and κ is a constant. An isothermal sphere has infinite mass, and cannot therefore describe a full cluster. It can be useful to describe the core of the cluster, since the inner regions can be considered to be nearly isothermal.

4. As the last model we mention the *lowered isothermal sphere*. This model adopts a velocity distribution function that allows to describe a finite cluster. Globular clusters have a finite radius since there is a maximum radius beyond which the tidal field of the Galaxy precludes bound orbits [10]. This radius is called *tidal-cutoff radius*. The velocity distribution function has the following shape:

$$f = \begin{cases} K\left(e^{-3E/\langle v^2 \rangle} - e^{-3E_e/\langle v^2 \rangle}\right) & \text{if } E < E_e \\ 0 & \text{if } E > E_e \end{cases}. \tag{2.9}$$

where E_e is the escape energy for a star in the cluster.

2.1.2 Evaporation

As we already mentioned globular clusters are finite systems, and the granularity of their gravitational field allows for a reshuffling of the magnitude and direction of the velocities of the stars in the cluster. This will drive the velocity distribution towards a Maxwellian distribution, and due to the high velocity tail of the Maxwellian and the constant reshuffling there will always be stars with enough energy to escape the cluster.

The mean energy per unit mass to remove a star from the cluster is defined as:

$$\frac{\langle v_e^2 \rangle}{2} \equiv \frac{\int \rho(r) v_e^2(r) dV}{2 \int \rho(r) dV}. \tag{2.10}$$

We now state that a star cluster can be considered as a *virialized system*, so the usual statement of the virial theorem applies:

$$2T = |W|, \tag{2.11}$$

where $T = \sum_{i=1}^{N} \frac{1}{2} m_i v_i^2$ and $W = -G \sum_{i=1}^{N} \sum_{j>i} \frac{m_i m_j}{|r_i - r_j|}$ are the kinetic and potential energy. Combining this with equation (2.10) we get that the velocity needed for a star to escape the cluster is:

$$\left\langle v_e^2 \right\rangle = 4 \left\langle v^2 \right\rangle. \tag{2.12}$$

A very rough estimate of the evaporation probability ξ_e can be obtained by assuming that the time to reshuffle the velocity of the stars to re-establish a Maxwellian is t_r (the *relaxation timescale*), and by considering the probability of evaporation proportional to the fraction of stars that have $v > 2v_e$ in a Maxwellian distribution:

$$\xi_e \propto 4\pi \int_{2v_m}^{\infty} f^{(0)}(v) v^2 dv, \tag{2.13}$$

and Spitzer [43] estimates that for a spherical uniform cluster $\xi_e = 7.4 \times 10^{-3}$. We can roughly estimate the evaporation time as:

$$t_{\text{evap}} \approx \frac{t_{\text{r}}}{\xi_e} = 136\, t_{\text{r}}, \tag{2.14}$$

which is longer than a Hubble time. Few globular clusters are therefore directly affected by evaporation, but the process can be accelerated by the presence of a tidal field, which can strip stars from the cluster. It is likely that the final fate of most globular cluster is the destruction due to tidal effects [4].

2.1.3 Gravothermal instability

Gravothermal instability is a process possible in an isothermal sphere such as the one described by eq. (2.8), confined within an outer, non isothermal envelope. These self-gravitating systems are characterized by a negative heat capacity, as a consequence of the virial theorem [43, 4]. As stars evaporate from the core into the outer envelope, the envelope increases its energy, acting as a heat sink for the core. On the other hand the core loses energy and will therefore contract, increasing the velocity dispersion of the stars in the core. If the core is large enough the increase in temperature is more significant in the envelope, and energy can flow back into the core, allowing for a state of stable equilibrium to exist [10]. Otherwise, if the core is small enough, the temperature gradient between the core and the envelope steepens indefinitely, as the contraction of the core accelerates. This runaway mechanism

causes the core to collapse. We can discuss this process with two approaches:

1. *Virial theorem approach:* as we mentioned the granularity of the gravitational field leads to the evaporation of the fastest stars from the core. This will cause a decrease in both K and $|W|$, but the evaporation will tend to break the virial equilibrium. In particular, since the fastest stars are lost, the decrease in K is bigger than that in $|W|$:

$$E_{tot,i} = K_i + W_i > E_{tot,f} = K_f + W_f, \tag{2.15}$$

   leading to a contraction of the core. The contraction of the core increases its temperature and its density, leading to more stars being expelled from it. In a real star cluster, this collapse can be halted, at least temporarily, thanks to the presence of binary systems that act as an energy reservoir for the cluster. We will explain this in more detail in the next chapter.

2. *Ideal gas approach:* we can show how self-gravitating systems have a negative heat capacity with an analogy with ideal gases. The kinetic energy of the system can be related to a dynamical temperature as [4]:

$$\frac{1}{2}m\langle v^2\rangle = \frac{3}{2}k_B T \tag{2.16}$$

   Combining this with the virial theorem ($E_{tot} = -K$) we can define the total energy of the systems as:

$$E_{tot} = -\frac{3}{2}Nk_B\langle T\rangle, \tag{2.17}$$

   Where N is the number of bodies in the system. The heat capacity is then:

$$C = \frac{dE}{d\langle T\rangle} = -\frac{3}{2}Nk_B. \tag{2.18}$$

   C is therefore always negative since N and k_B are positive constants.

Chapter 3

Binary system dynamics

Dense star clusters, as we mentioned in the previous chapter, are *collisional systems*. In a collisional system close encounters between stars are possible and relevant with respect to the lifetime of the system. As we mentioned in the previous chapter, the two-body relaxation timescale is defined as [26, 42]:

$$t_{\mathrm{r}} = 0.34 \frac{\sigma^3}{G^2 \langle m \rangle \rho \ln(0.4N)}, \tag{3.1}$$

where σ is the velocity dispersion of the stars in the star cluster, $\langle m \rangle$ is the average mass of the stars, ρ is the local mass density and N is the number of stars in the cluster. Since for globular clusters t_{r} amounts to roughly $10^9 yr$ [36], they can be considered collisional systems.

Since a vast portion of the stars in the field, if not the majority, lives in a multiple system [15], we can expect the interaction between binaries and single stars in the cluster to be a relevant process.

A binary has internal energy given by:

$$E_{\mathrm{int}} = \frac{1}{2}\mu V^2 - \frac{G m_1 m_2}{r}, \tag{3.2}$$

where $\mu = (m_1 m_2) / (m_1 + m_2)$ is the reduced mass and V is the relative velocity between the two bodies and r is their distance. We can also define the binding energy of the binary as:

$$E_{\mathrm{bin}} = \frac{G m_1 m_2}{2a} = -E_{\mathrm{int}}, \tag{3.3}$$

where a is the semi-major axis.

We can classify binaries comparing their binding energy to the average kinetic energy of the stars in the cluster.

- *Hard binaries*: we call hard binaries those that have a higher binding energy compared to the average kinetic energy of the stars in the cluster:

$$E_{bin} > \frac{1}{2}\langle m \rangle \sigma^2; \tag{3.4}$$

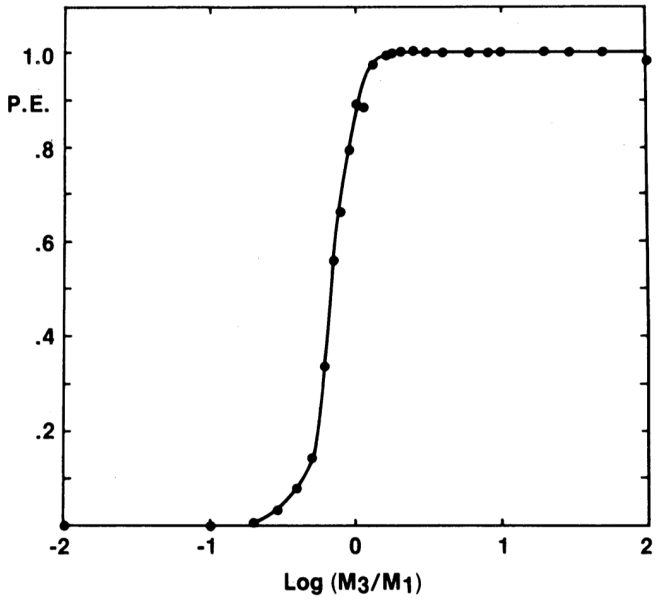

Figure 3.1: Exchange probability as a function of the mass ratio m_3/m_1 [21].

- *Soft binaries*: we call soft binaries those that have a lower binding energy compared to the average kinetic energy of the stars in the cluster:

$$E_{bin} < \frac{1}{2}\langle m \rangle \sigma^2, \tag{3.5}$$

where $\langle m \rangle$ is the average mass of a star in the cluster and σ is their velocity dispersion.

3.1 Three-body encounters

A *three-body encounter* is a close encounter between a binary and a field star in a star cluster, that allows for some energy to be exchanged between the binary and the single star. Following [23, 41] we can classify a three-body encounter in the following way, based on its outcome. In this classification we do not consider the possibility of two stars merging since it is not relevant in the context of this work.

- The first possibility is the so called *flyby interaction*. In this type of process the field star interacts with the binary and escapes, leaving the binary bound at the end of the interaction. The binary after the interaction will have of course different properties, but it will still be made of the same two bodies. This can happen for any amount of the total energy of the system.
- The second possibility is the so called *exchange*. This interaction is similar to the flyby, i.e. the outcome of the interaction is still a bound binary and a star that escapes. In this case though, the field star forms a new binary with one of the components of the original binary, while the other component

escapes. This too can happen for any amount of the total energy of the system. The probability of an exchange is strongly dependent on the mass ratio between the incoming star and the binary components [21]. Fig. 3.1 shows the probability of an exchange as a function of the mass ratio $m_3/m_{1,2}$. The probability is very close to zero for $m_3/m_{1,2} < 0.2$, and approximates unity for $m_3/m_{1,2} > 1.6$.

- The third possibility is the so called *ionization*. In this case all the stars become unbound after the interaction, and escape to infinity in different directions. This can happen only if the total energy is positive. In particular we can compute a critical velocity for the intruder, below which it doesn't have enough energy to ionize the system. To compute this threshold velocity we need to impose the condition $\mu V_c/2 = E_{bin}$, getting:

$$V_c^2 = \frac{2\,(m_1 + m_2 + m_3)\,E_{bin}}{m_3\,(m_1 + m_2)}. \tag{3.6}$$

We can also consider a second classification, not based on the outcome of the process but on what happens during the encounter. In fact during a three body interaction the stars can temporarily form a bound three body system, which will eventually decay in a flyby interaction or an exchange. If this occurs the interaction is called a *resonant scattering* (either a *resonant flyby* or a *resonant exchange*). Otherwise we refer to a *prompt interaction* (*prompt flyby*, *prompt exchange*, ionization). An operative way to determine which of these two types of interaction occurs is explained in [23]. They define a resonant interaction one in which the mean square distance, defined as:

$$s(t) = \left[\frac{1}{3}\sum_{i<j} |r_i(t) - r_j(t)|^2\right]^{1/2}, \tag{3.7}$$

has more than one minimum during the interaction. If instead the minimum is only one, than the interaction is prompt. The rates of these processes are described by differential cross sections, and we discuss them in chapter 5. In fig. 3.2 the cross sections for exchange, ionization and resonant processes as a function of the velocity of the intruder are shown, for binaries with eccentricity $e = 0.7$.

3.1.1 Dynamical Hardening

Heggie's law states that, as a consequence of three-body interactions, hard binaries tend to become harder (i.e. increase their binding energy), while soft binaries tend to become softer (i.e. decrease their binding energy) [16]. The dynamical hardening process is particularly relevant for binary black holes (BBHs), since black holes are among the most massive objects in star clusters [4] and therefore BBHs are usually hard binaries [26, 40]. Dynamical hardening is responsible for the shrinking of BBHs semi-major axis to the point where they enter the regime of gravitational

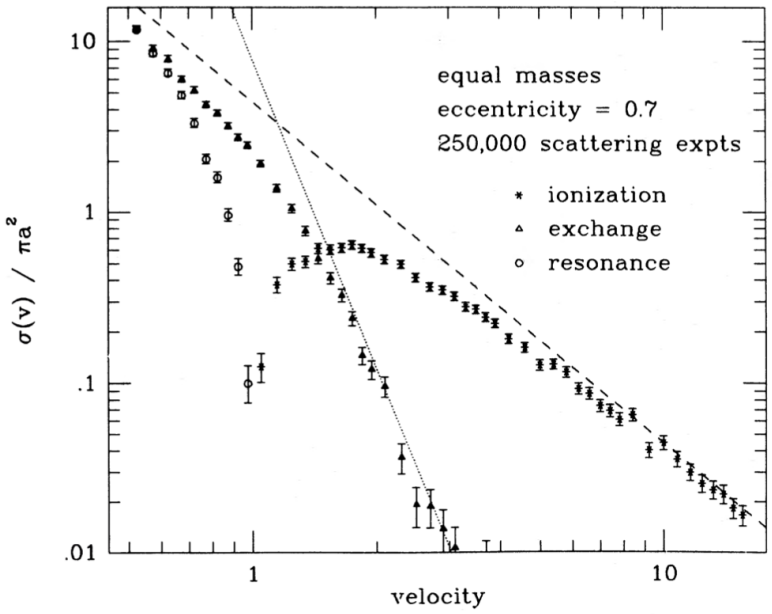

Figure 3.2: Cross sections for exchange, resonance and ionization as a function of the velocity of the intruder for binaries with $e = 0.7$ [23].

wave emission. Without dynamical hardening the predicted merger rate of BBHs would be too low to be detected [35]. We will treat this process in more detail in section 5.1.

The process of dynamical hardening is relevant also for the evolution of the star cluster itself. As we saw in chapter 2, globular clusters can undergo a process of core collapse, called gravothermal catastrophe. The collapse can though be halted, at least temporarily, by an energy source in the core. The energy needed is provided by hardening of tight binaries. Single stars in the core scatter off these binaries, gaining kinetic energy by extracting it from the orbital energy of the binary, allowing the core of the star cluster to return in equilibrium or even start to expand again. In analogy to nuclear burning in stars, that allows them to be in equilibrium, this process is called *binary burning* [4].

3.1.2 Gravitational focusing

A relevant process that has to be discussed when considering three-body encounters is that of *gravitational focusing*. This process is responsible for the deflection of the trajectory of the field star as it approaches the binary, due to the gravitational pull between the binary and the single star. The result of this is that the distance of closest approach between the binary and the field star will be less than the impact parameter at infinity. Let's compute the cross-section for a field star to pass within a distance r_{min} from the center of gravity of the binary [43]. We approximate the binary as a sphere of mass M, m_3 is the mass of the intruder and b is the impact parameter of the intruder with respect ti the binary at infinity, such that the pericenter of the orbit of m_3 is r_{min}. $V(r)$ is the relative velocity between the

binary and intruder at a given separation. We can write the conservation laws for the angular momentum and the energy:

$$bV(r \to \infty) = r_{\min} V\left(r_{\min}\right), \tag{3.8}$$

$$\frac{1}{2}\mu V(r \to \infty)^2 = \frac{1}{2}\mu V\left(r_{\min}\right)^2 - \frac{G m_3 M}{r_{\min}}, \tag{3.9}$$

where $\mu = m_3(m_1+m_2)/(m_1+m_2+m_3)$ is the reduced mass for the relative motion of the single star with respect to the binary. Solving for b and inserting it in the expression for the cross section we get:

$$\sigma = \pi b^2 = \pi r_{\min}^2 \left[1 + \frac{2G\left(M + m_3\right)}{r_{\min} V(r \to \infty)^2}\right]. \tag{3.10}$$

3.2 Thermal eccentricity distribution

In 1919 Jeans discovered that if a population of binaries is *thermalised* the eccentricity distribution for the binaries can be described by the following equation [24, 16]:

$$f(e)\, de = 2e\, de, \tag{3.11}$$

and therefore all values of e^2 are equally likely. The thermalization condition is satisfied when the population of binaries reaches a state of statistical equilibrium, which approximates energy equipartition. The distribution of energies for such a system will follow a Boltzmann distribution. Such a state of equilibrium can be reached if the binaries have all interacted with each other through dynamical encounters, and have therefore exchanged energy many times. This distribution for the eccentricities has been widely used when determining the initial conditions in theoretical investigations of binary systems [11].

Since deriving eq. (3.11) considering a Boltzmann distribution for the binding energies of the binaries is quite involved, here we show how to obtain the same result considering a uniform distribution for the binding energies, following [25]. We start consindering the Keplerian orbital angular momentum for a bound two body system:

$$L = \mu\sqrt{GMa\left(1 - e^2\right)}, \tag{3.12}$$

where $\mu = (m_1 m_2)/(m_1 + m_2)$ is the reduced mass, $M = m_1 + m_2$ is the total mass and a the semi-major axis of the binary. We consider also the binding energy of the binary:

$$E_b = \frac{G m_1 m_2}{2a}. \tag{3.13}$$

Combining eq. (3.12) and eq. (3.13) we can write:

$$L^2 = \frac{G}{m_{\rm sys}} \frac{G m_1 m_2}{2E_{\rm bin}} \left(1 - e^2\right) \left(m_1 m_2\right)^2. \tag{3.14}$$

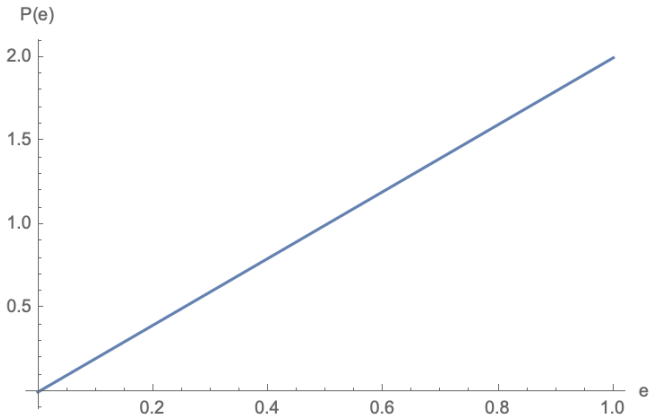

Figure 3.3: The thermal eccentricity distribution.

We can therefore write an expression for the eccentricity e as a function of the binding energy E_b:

$$e = \left(1 - 2E_{\text{bin}}L^2\frac{m_{\text{sys}}}{G^2\left(m_1m_2\right)^2}\right)^{\frac{1}{2}}. \tag{3.15}$$

Differentiating with respect to E_{bin} we get:

$$\frac{de}{dE_{\text{bin}}} = \left[-L^2\frac{m_{\text{sys}}}{G^2\left(m_1m_2\right)^2}\right]e^{-1}. \tag{3.16}$$

Now, since the fraction of binaries in the range $e, e+de$ is equal to the fraction of binaries in the range $E_{\text{bin}}, E_{\text{bin}}+dE_{\text{bin}}$:

$$f(e)de = f\left(E_{\text{bin}}\right)dE_{\text{bin}} = f\left(E_{\text{bin}}\right)\left[-L^2\frac{m_{\text{sys}}}{G^2\left(m_1m_2\right)^2}\right]^{-1}e\,de \equiv K\,e\,de. \tag{3.17}$$

Since we want:

$$\int_0^1 f(e)de = 1, \tag{3.18}$$

we have can compute the value of K and the shape of $f(e)$:

$$1 = K\int_0^1 e\,de \Longrightarrow K = 2 \Longrightarrow f(e)\,de = 2e\,de. \tag{3.19}$$

The distribution is shown in fig. 3.3

3.3 BBH mergers in globular clusters

Estimates suggest that from 10^{-4} to less than 10^{-6} stars will end up as black holes. The same can be expected to happen in globular clusters. Since they contain about 10^6 stars we can expect between zero and 100 black holes to live in a globular

cluster [40]. These heavy objects tend to sink towards the core of the cluster as a consequence of a process called *dynamical friction* [5]. It is a consequence of gravity force that produces a drag force on a heavy body moving in a sea of lighter particles. Qualitatively this happens because, as the heavy body moves, it attracts lighter bodies, leaving a slight overdensity of matter behind. This overdensity attracts the heavy body and is responsible for its deceleration. The deceleration happens on the *dynamical friction timescale* $t_{\rm DF}$ [26]:

$$t_{\rm DF}(M) = \frac{3}{4(2\pi)^{1/2} G^2 \ln\Lambda} \frac{\sigma^3}{M\rho(r)}, \tag{3.20}$$

which is typically a small fraction of the relaxation timescale. As a dense population of stars, globular clusters host many dynamical interactions between stars, particularly in their core, where heavy objects sink. These dynamical interactions enhance the production of relativistic binaries, driving binaries towards tighter orbits, favouring the exchange of the binary components towards heavier objects [4]. Globular clusters have an enhanced efficiency for the production of binary black holes (BBHs) due to their dynamics, allowing for many-body interactions [3]. As we saw, dynamical interactions between BBHs and stars in the cluster tend to decrease the semi-major axis of the binary, allowing them to enter the gravitational wave regime faster and therefore merge. Even though the majority of the BBHs are ejected from the cluster before merging, a fraction can merge inside the cluster. Askar et al. [3] estimated the local merger rate density for BBHs considering both escaping binaries and binaries that merge in the cluster to be $\mathcal{R} = 5.4 \mathrm{Gpc}^{-3}\mathrm{yr}^{-1}$.

Chapter 4

RESULTS: Modelling binary-single encounters with the direct N-body code ARWV

In the second part of my thesis, my goal is to show that the eccentricity of a single hard binary tends to increase after a set of three-body encounters. I obtained this result by means of three-body encounters with the direct N-body code ARWV. I chose this code since it allows to integrate the orbits of the bodies involved in the encounters with high precision, thanks to features such as the algorithmic regularization and a chain structure.

4.1 ARWV

ARWV is a high-precision direct N-body code intended to integrate a few-body problem ($N \leq 500$) via the use of *chained variables* for the coordinates and velocities of stellar bodies [7, 6]. It is an updated and modified version of the algorithmic regularization chain code by Seppo Mikkola [29]. ARWV is able to model systems with arbitrary mass ratios even for long periods of time.

4.1.1 Chain structure

ARWV uses a chain structure to minimize round off errors. These errors can be a major problem when a close encounter takes place and the coordinates of the bodies involved are measured from a distant origin. The chain structure consists in a rule to assign an index to each body in the simulated system, affecting the way in which positions and velocities of the bodies are stored by the code. Using a standard approach the position and velocities of N bodies could be stored in an array of size $6N$. These positions and velocities could be computed with respect to the center of mass of the system, and stored considering an arbitrary indexing of the bodies. ARWV instead, to assign an index to each body, begins by choosing randomly a first body. This body will be used as a reference becoming the origin

of the chain. The other bodies are numbered as to minimize the distance between any given member of the chain and the next one. So for any ith element of the chain, the element $(i+1)$th will be chosen as the closest to ith the element. This is repeated until a chain including all the bodies in the system is obtained. Positions and velocities of the bodies in the system are then stored in an array with size $6(N-1)$, since the first body represents the origin of the coordinates. In practice this is achieved by sorting all the distances between particles, and searching among the still unused distances to find to next closest body, until the chain is completed. The chain is upgraded after every integration step.

4.1.2 Algorithmic regularization

The relative acceleration induced by point-like bodies in the case of close encounters can grow enormously, due to the $1/r$ dependence of the Newtonian gravitational potential. Close encounters can therefore lead to the UV divergence of the Newtonian potential, which would cause a 'classic' integration algorithm to fail. ARWV can *regularize* the close encounters by a proper computation of coordinates and velocities, which is performed by the leapfrog algorithm. Although ARVW implements different regularization methods, which can also be used in combination [7], for this work I used the *logarithmic-Hamiltonian* (logH) method [29, 30]. This method is based on the definition of a time transformation for the leapfrog integrator. The logarithmic Hamiltonian is defined as:

$$\Lambda = \ln(T+B) - \ln(U), \tag{4.1}$$

where $T = \sum_{k=1}^{N} \mathbf{p}_k^2/2m_k$ is the kinetic energy, $U = \sum_{0<i<j\leq N} m_i m_j/\left|\mathbf{r}_i - \mathbf{r}_j\right|$ is the potential energy and B is the momentum associated to the time coordinate (or binding energy), since we are considering an extended phase space. The index $k = 1, ..., N$ refers to the bodies present in the simulation. The functions T and U are such that $H = T - U$ is the usual Hamiltonian. The logarithmic Hamiltonian gives the following equations of motion [29, 31]:

$$t' = \frac{\partial \Lambda}{\partial B} = 1/(T+B), \tag{4.2}$$

$$\mathbf{r}_k' = \frac{\partial T}{\partial \mathbf{p}_k}/(T+B), \tag{4.3}$$

$$B' = \frac{\partial U}{\partial t}/U, \tag{4.4}$$

$$\mathbf{p}_k' = \frac{\partial U}{\partial \mathbf{r}_k}/U, \tag{4.5}$$

where eq. (4.4) is needed only if a time-dependent potential is added. Since the right hand sides of these equations do not depend on the left hand side variables, it is possible to build a leapfrog algorithm. Here we consider the leapfrog scheme in the drift-kick-drift (DKD) declination, where we first advance the position by half

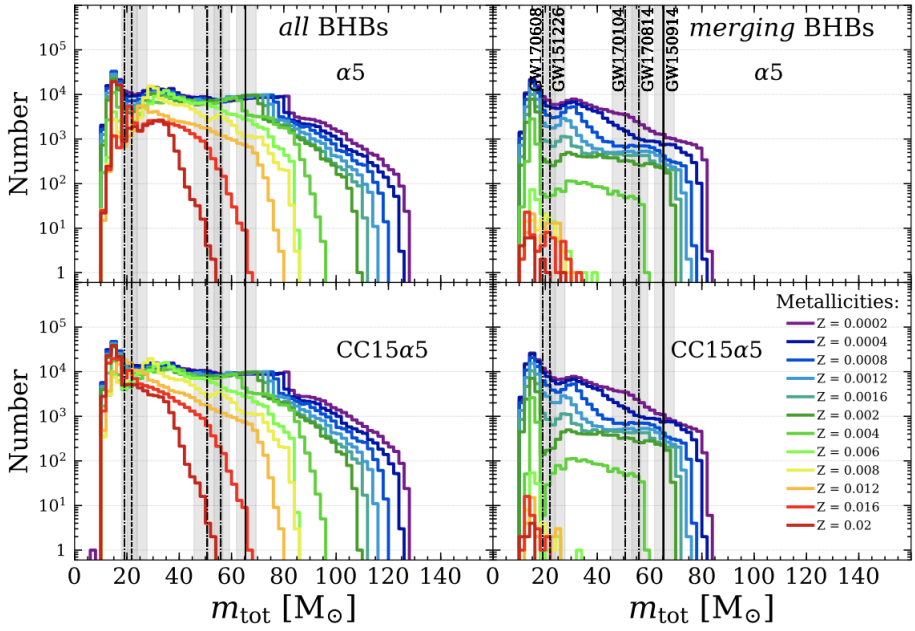

Figure 4.1: Distribution of total masses of BBHs simulated with MOBSE, for different initial conditions for the MOBSE simulations [12]. We refer to the top-left panel, where all the BBHs formed in the simulation are shown, and we selected $Z = 0.002$.

a time step, then the velocity to the end of the time step and finally the position to the end of the time step. Considering a time step of size h we have:

$$\delta t = \frac{h/2}{T+B}, \quad t \to t+\delta t, \quad \mathbf{r}_k(h/2) = \mathbf{r}_k(0) + \delta t \frac{\partial T}{\partial \mathbf{p}_k}(0), \tag{4.6}$$

then:

$$\delta t = \frac{h}{T+B}, \quad B(h) = B(0) + \delta t \frac{\partial U}{\partial t}(0), \quad \mathbf{p}_k(h) = \mathbf{p}_k(0) + \delta t \frac{\partial U}{\partial \mathbf{r}_k}(0), \tag{4.7}$$

and finally:

$$\delta t = \frac{h/2}{T+B}, \quad t \to t+\delta t, \quad \mathbf{r}_k(h) = \mathbf{r}_k(h/2) + \delta t \frac{\partial T}{\partial \mathbf{p}_k}(h). \tag{4.8}$$

4.2 Initial conditions

Each of our synthetic three-body systems is composed of an *initial binary* (m_1, m_2) and of an *intruder* (m_3). For the equal mass case I set $m_1 = m_2 = m_3 = m = 10M_\odot$. For the unequal mass case the masses of each component (m_1, m_2, m_3) are sampled individually from a distribution of BBH masses obtained with the

population synthesis code MOBSE (fig. 4.1, [12, 13]). This distribution is the result of the simulation of 10^7 binary systems with metallicity $Z = 0.002 \simeq 0.1 Z_\odot$, and includes both interacting and non interacting BBHs. If the BHs in the binary interact, both surviving and merging BBHs are included. In this way it is possible to account for the lack of stellar and binary evolution in ARWV.

The initial eccentricity e of each initial binary is sampled randomly from a thermal distribution, which is uniform in e^2 in the interval [0,1) [16].

In the equal mass case the initial semi-major axis is computed as:

$$a = \frac{Gm}{2\sigma^2}, \tag{4.9}$$

where σ is the three-dimensional velocity dispersion of stars in the star clusters. The initial binaries will thus be at the hard-soft boundary (will be better explained in the previous chapter).

For the unequal mass case, the initial semi-major axis a of each initial binary is randomly sampled from a log-normal distribution with $\mu_{\log} \simeq 1.22\,\mathrm{AU}$ and $\sigma_{\log} \simeq 0.92\,\mathrm{AU}$. This choice comes from the typical properties of black hole binaries formed in simulations in [9]. The sample is then accepted if $a \in [\max(a_{\rm ej}, a_{\rm gw}), a_{\rm hard}]$, otherwise it is rejected and sampled again. $a_{\rm ej}$ is the semi-major axis below which the binary can be ejected from the star cluster by a single-binary scattering event and it is defined as [8]:

$$a_{\rm ej} = \frac{\xi m_3^2}{(m_1+m_2)^3}\frac{G m_1 m_2}{v_{\rm esc}^2}, \tag{4.10}$$

where $v_{\rm esc}$ is the escape velocity from the star cluster and $\xi = 3$ is a numerically calibrated dimensionless parameter. $a_{\rm gw}$ is the semi-major axis below which the main gravitational wave emission becomes the main driver of the orbital decay, instead of dynamical hardening, and it is given by [28]

$$a_{\rm GW} = \left[\frac{32 G^2}{5\pi\xi c^5}\frac{\sigma m_1 m_2 (m_1+m_2)}{\rho_{\rm c}(1-e^2)^{7/2}}\left(1+\frac{73}{24}e^2+\frac{37}{96}e^4\right)\right]^{1/5}, \tag{4.11}$$

where σ is the 3D velocity dispersion for stars in the cluster and $\rho_{\rm c}$ is the core mass density. $a_{\rm hard}$ is the maximum a for the binary to be hard:

$$a_{\rm hard} = \frac{G m_1 m_2}{\langle m\rangle \sigma^2}. \tag{4.12}$$

This method allows us to generate hard initial binaries that will not merge nor get expelled from the star cluster.

The asymptotic incoming velocity of the intruder with respect to the initial binary is randomly drawn form a Maxwellian distribution, given by

$$p(v)\mathrm{d}v = \sqrt{\frac{2}{\pi}}\frac{v^2}{\sigma^3}\exp\left(-\frac{v^2}{2\sigma^2}\right)\mathrm{d}v, \tag{4.13}$$

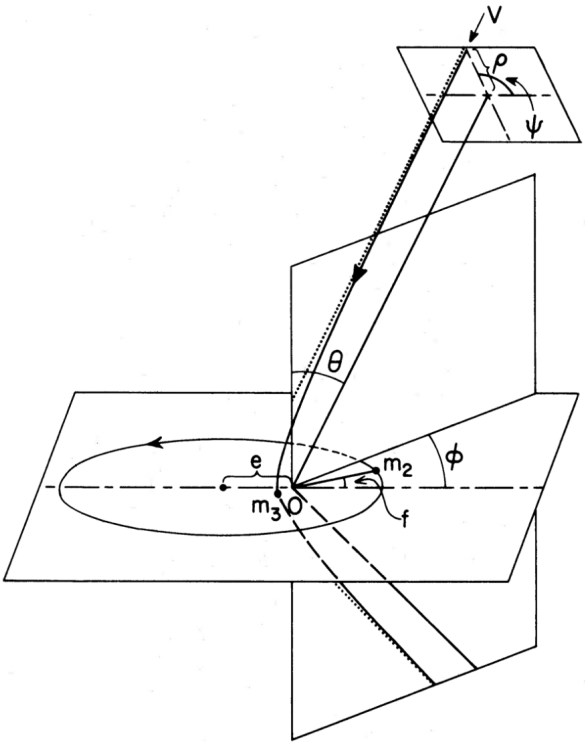

Figure 4.2: Parametrization of initial values for the scattering of an intruder off a binary. [23]

with dispersion $\sigma = 10\sqrt{3/2}\,\mathrm{kms}^{-1}$. This distribution can be randomly sampled as $v = \sqrt{x^2 + y^2 + z^2}$, where x, y and z are three Gaussian random numbers, with a probability distribution function centered in zero and with the same σ.

The initial distance between the intruder and the initial binary is given by $D = 10^3 a$ for each system, so that the initial binary is initially unperturbed.

The remaining initial quantities (orbital phase f, the three orientation angles θ, ϕ, ψ and the impact parameter b) are defined and sampled following [23], and can be seen in fig 4.2. Since there is no explicit expression for $f(t)$ we need to solve Kepler's equation:

$$\frac{2\pi}{T} t = E - e \sin E, \tag{4.14}$$

where t is the time since periastron passage, T is the orbital period and E is the eccentric anomaly. E is related to the phase f by

$$\tan\left(\frac{f}{2}\right) = \left(\frac{1+e}{1-e}\right)^{1/2} \tan\left(\frac{E}{2}\right). \tag{4.15}$$

To determine the phase f we first draw a uniform random number in the interval $[0, 2\pi)$ as the value of $E - e \sin E$. E is then approximated using the bisection method, and the value of f is obtained from eq. (4.15). This allows to give every angular element a weight equal to the fraction of the time which the system spends in that part of the orbit.

θ is the angle between the versor perpendicular to the orbital plane of the binary and the velocity vector of the intruder at infinity, and it is sampled uniformly from $\cos\theta$ in $[-1, 1]$; ϕ is the angle between the pericentre direction on the orbital plane and the intersection of the orbital plane with the plane in which the initial velocity vector of the intruder lies, and it is sampled uniformly in $[0, 2\pi)$; ψ is the angle, defined on a plane perpendicular to the velocity vector, between the orientation of the impact parameter and the orbital plane direction, and it is sampled uniformly in $[0, 2\pi)$.

Finally, the impact parameter b is sampled according to an equal probability distribution in b^2, hence proportional to the area of a surface element perpendicular to the direction of the velocity of the intruder. The values of b are generated in the interval $[0, b_{\max}]$, where the upper limit for a hard encounter is derived from the gravitational focusing expression [8]:

$$b_{\max} = \frac{\sqrt{2G\left(m_1 + m_2 + m_3\right) a}}{v_\infty}. \tag{4.16}$$

We also ensure that $b < 10^2 a$ per each encounter, in order to exclude soft encounters from our simulations. Soft encounters are characterized by a negligible energy exchange between the intruder and the binary, thus leaving the configuration of the system unchanged.

4.3 The scattering experiments

I simulated the evolution of 10^3 initial equal mass binaries and 10^3 initial unequal mass binaries undergoing at most 8 scattering events with an intruder. The possible outcome of one of these three-body encounters is either a flyby, an exchange or an ionization (these possibilities will be explained in detail in another chapter). Each three body encounter is integrated for 10^5yr. If the encounter does not lead to the disruption of the binary (ionization), a new encounter is performed, where the binary at the last time step of the previous simulation is used as the initial binary of the new simulation. New intruder properties are sampled as in section 4.2, and the system is integrated. This is repeated for a maximum of 8 encounters per initial binary. I call nth *generation* the group of systems that has undergone n scattering events. At the end of each encounter I check if the three-body interaction is still ongoing by looking at the binding energy associated to each possible couple. If two or more couples are still gravitationally bound, the system is integrated for another 10^5yr, until the interaction is completed (with a BBH and a single unbound BH left or three single unbound BHs left).

In fig. 4.3 and in fig. 4.4 I show the evolution of the eccentricity distribution for the 8 generations for the equal and unequal mass cases. Figure 4.3 highlights a tendency of the eccentricity distribution to drift towards a super-thermal distribution, in particular for the equal mass case. The top-left panels of fig. 4.4 show the starting eccentricity distributions, which are thermal, and as more scattering events happen more systems move to high eccentricity bins, as is showed by the

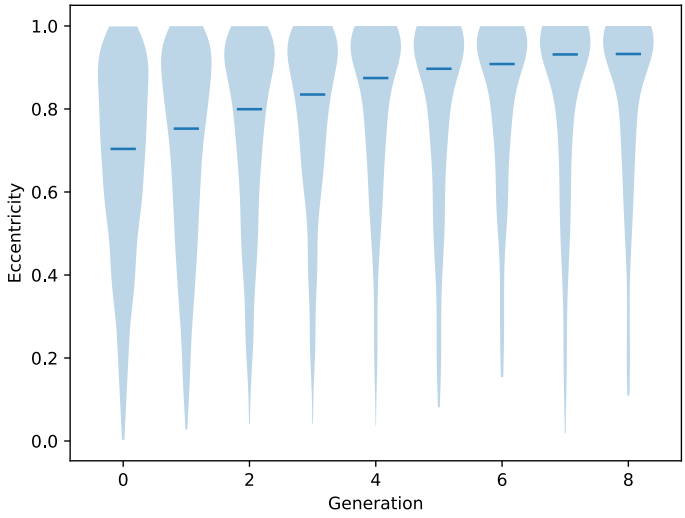

(a) Equal mass case

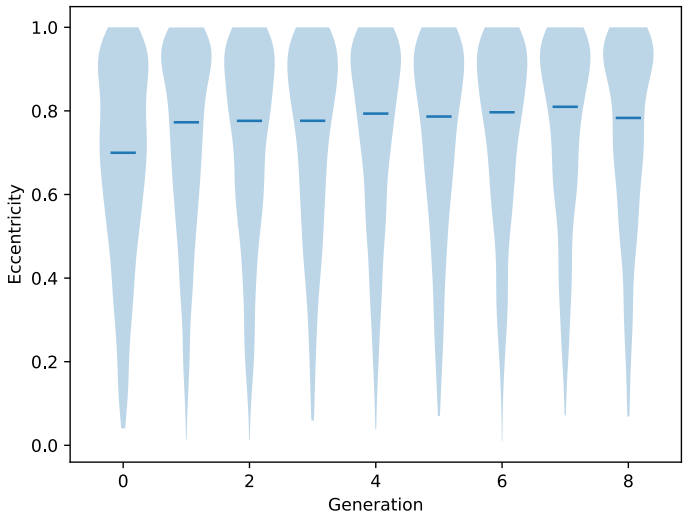

(b) Unequal mass case

Figure 4.3: Violin plots showing the eccentricity distributions for different generations. In the top panel we show the evolution of the eccentricity distribution for the equal mass case, while in the bottom panel we show the evolution of the eccentricity distribution for the unequal mass case. The median values of each distribution are highlighted.

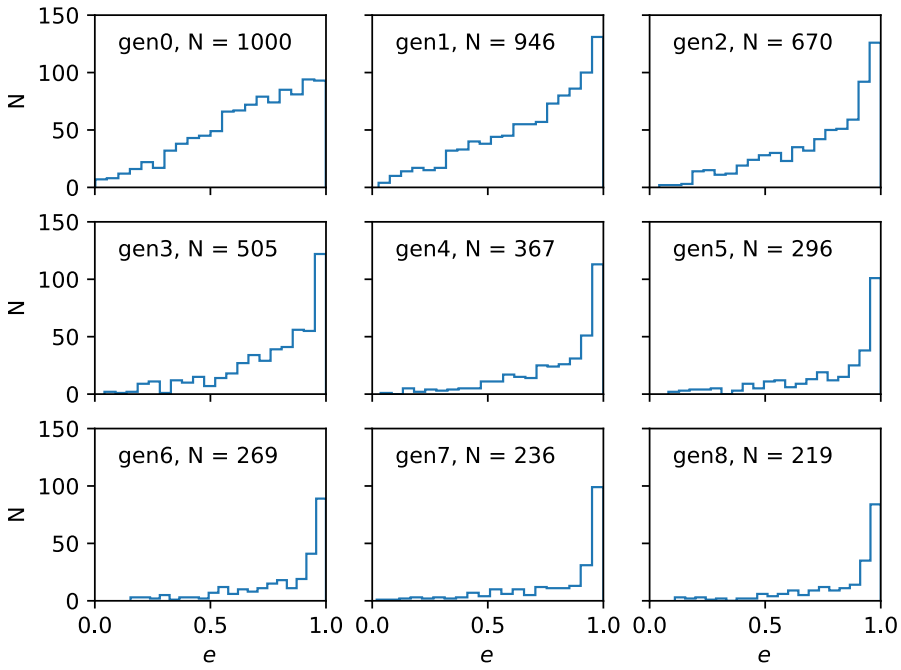

(a) Equal mass case

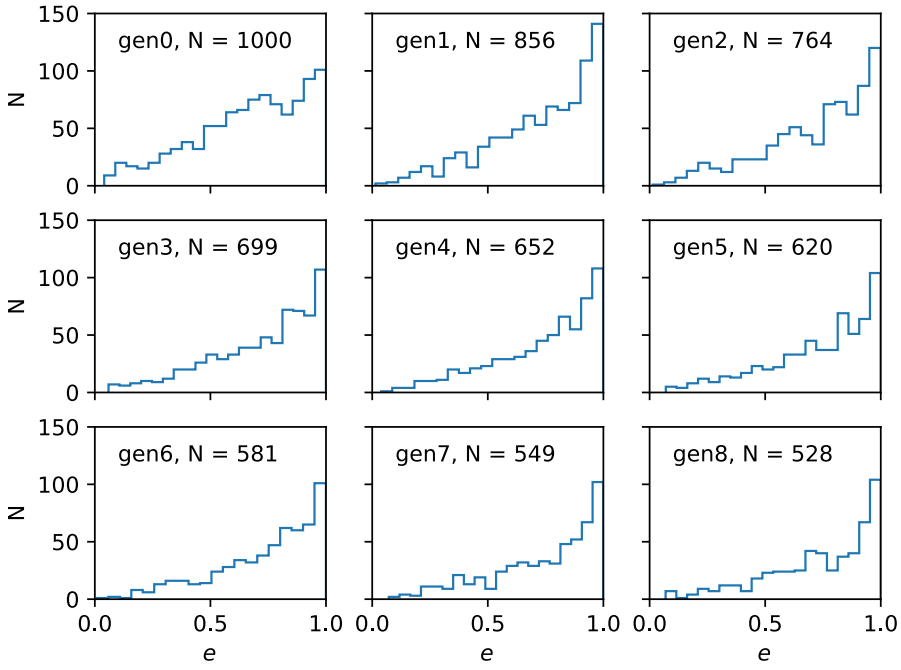

(b) Unequal mass case

Figure 4.4: Histograms showing the eccentricity distribution per generation for the equal mass and unequal mass cases. Also the total number of binaries present per generation is showed.

	gen 1	gen 2	gen 3	gen 4	gen 5	gen 6	gen 7	gen 8	average
equal mass	5.4%	29.2%	24.6%	27.3%	19.3%	9.1%	12.2%	7.2%	32.2%
unequal mass	14.4%	10.7%	8.5%	6.7%	4.9%	6.3%	5.5%	3.8%	7.6%

Table 4.1: Fraction of ionized systems after each generation and averaged over all generations for equal and unequal mass cases.

	gen 0	gen 1	gen 2	gen 3	gen 4	gen 5	gen 6	gen 7	gen 8
median e	0.70	0.75	0.80	0.83	0.87	0.90	0.91	0.93	0.93
$e > 0.9/e_{\rm tot}$	0.19	0.25	0.34	0.36	0.46	0.48	0.52	0.55	0.57

Table 4.2: Values of the median e and the fraction of systems with $e > 0.9$ per each generation in the equal mass case.

other panels.

In fig. 4.4 the number of systems present in each generation is also shown. This number decreases as the generation increases because a fraction of binaries is ionized by the interaction with the intruders. The fraction of ionized systems per generation and averaged over all generations are showed in tab. 4.1, for both the equal and unequal mass cases.

The thermal distribution has a median eccentricity of 0.7 and the probability of having an $e > 0.9$ associated to this distribution is 0.19. The median values of the eccentricity distributions at each generation and the fraction of systems with $e > 0.9$ at each generation for the equal mass case are shown in tab. 4.2, and for the unequal mass case in tab. 4.3.

For the equal mass case, after each initial binary has undergone the first scattering event the median value of the eccentricity distribution increases by $\sim 7\%$. The average increase in the median of the eccentricity distribution considering all the 8 generations is $\sim 3.5\%$. Again for the equal mass case, after each initial binary has undergone the first scattering event, the fraction of systems with $e > 0.9$ increases by $\sim 32\%$. The average increase in the fraction of systems with $e > 0.9$ considering all the 8 generations is $\sim 15\%$. For the unequal mass case the increase in the median value of the eccentricity distribution for the first generation is $\sim 10\%$, while the average increase in the median of the eccentricity distribution over all the 8 generations is $\sim 1\%$. Again for the unequal mass case, the increase in the fraction of systems with $e > 0.9$ for the first generation is $\sim 45\%$, while the average increase

	gen 0	gen 1	gen 2	gen 3	gen 4	gen 5	gen 6	gen 7	gen 8
median e	0.70	0.77	0.78	0.78	0.79	0.79	0.78	0.81	0.78
$e > 0.9/e_{\rm tot}$	0.20	0.29	0.27	0.26	0.30	0.28	0.29	0.32	0.34

Table 4.3: Values of the median e and the fraction of systems with $e > 0.9$ per each generation in the unequal mass case.

	gen 1	average over all generations
increase in median e wrt gen 0	$\sim 7\%$	$\sim 3.5\%$
increase in the fraction of systems with $e > 0.9$ wrt gen 0	$\sim 32\%$	$\sim 15\%$

Table 4.4: Increase of the median e and of the fraction of systems with $e > 0.9$ with respect to the 0-th generation for the 1-st generation and averaged over all generations. Case of equal masses.

	gen 1	average over all generations
increase in median e wrt gen 0	$\sim 10\%$	$\sim 1\%$
increase in the fraction of systems with $e > 0.9$ wrt gen 0	$\sim 45\%$	$\sim 7.7\%$

Table 4.5: Increase of the median e and of the fraction of systems with $e > 0.9$ with respect to the 0-th generation for the 1-st generation and averaged over all generations. Case of unequal masses.

in the fraction of systems with $e > 0.9$ over all the 8 generations is $\sim 7.7\%$. These numbers are summarized in tab. 4.4 and tab. 4.5. Ginat and Perets in [14] found a super-thermal eccentricity distribution with a probability for $e > 0.9$ of 0.22, an increase of $\sim 15\%$ with respect to a thermal distribution.

Fig. 4.4 shows how not only the ratio, but also the number of systems with $e > 0.9$ increases after the first scattering event, despite having less systems overall because of ionization. The number of systems with $e > 0.9$ for the equal mass case before any scattering event is 186, which increases to 236 for the first generation. In the unequal mass case, the initial number of systems with $e > 0.9$ is 200, which increases to 252 for the first generation. The plots in fig. 4.5 show in more detail how systems change their eccentricity going from the zeroth generation to the first. The top panel shows the equal mass systems while the bottom panel shows the unequal mass systems. In both panels the black histogram shows the total eccentricity distribution at the first generation; the blue histogram shows the final e of systems that had $e < 0.9$ at the zeroth generation and that after the first scattering drifted to a higher $e > 0.9$; the green histogram shows the e of the systems that started with $e > 0.9$ and drifted to a lower $e < 0.9$; the yellow histogram shows the starting eccentricity (at the zeroth generation) of the systems that ended up with $e > 0.9$ at the first generation (blue histogram); the red histogram shows the eccentricity of systems that after the scattering retained a $e > 0.9$.

As a test I also ran two smaller scale equal mass simulations with 10^2 systems considering two different starting distributions for the eccentricity: an initial uniform distribution in the interval [0,1] and an initial distribution for low eccentricity, uniform in the interval [0,0.1]. The results are shown in fig. 4.6. In both cases the eccentricity distribution drifts towards higher values of e. Bigger fluctuations are due to the smaller size of the samples.

Figure 4.8 shows the evolution of the eccentricity distributions for the unequal mass case as a function of the semi-major axis of the binary in the top panel and

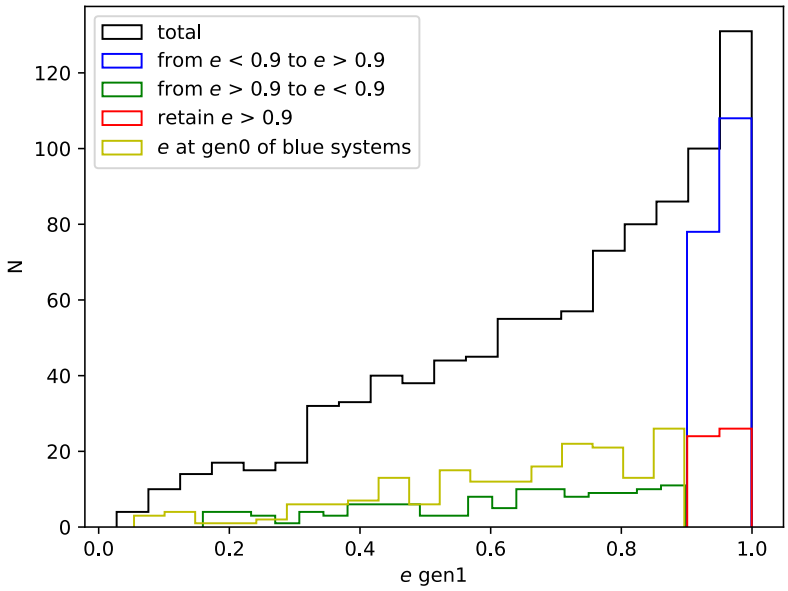

(a) Equal mass case

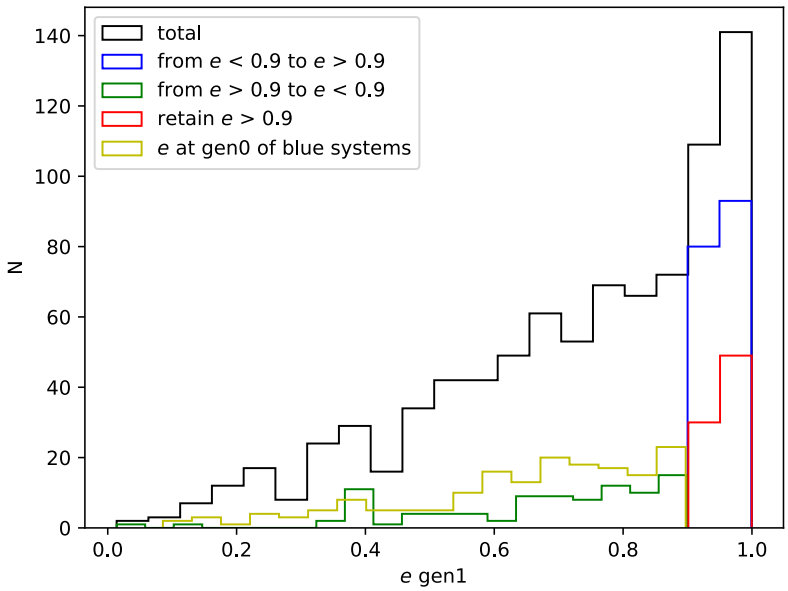

(b) Unequal mass case

Figure 4.5: Histograms showing the detail of how systems change their eccentricity going from the zeroth generation to the first generation. The equal mass case is on the top panel, the unequal mass case on the bottom panel.

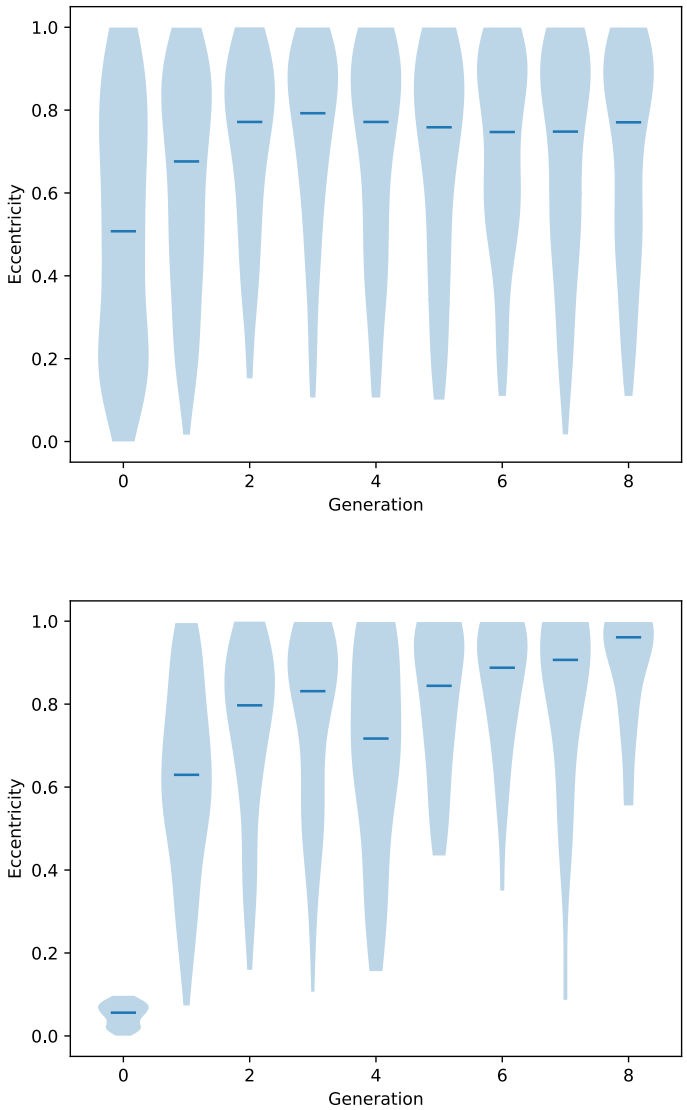

Figure 4.6: Violin plots showing the eccentricity distribution evolution for different initial distributions. In the top panel the initial distribution for e is uniform in the interval [0,1], while in the bottom panel the initial distribution is uniform in the interval [0,0.1].

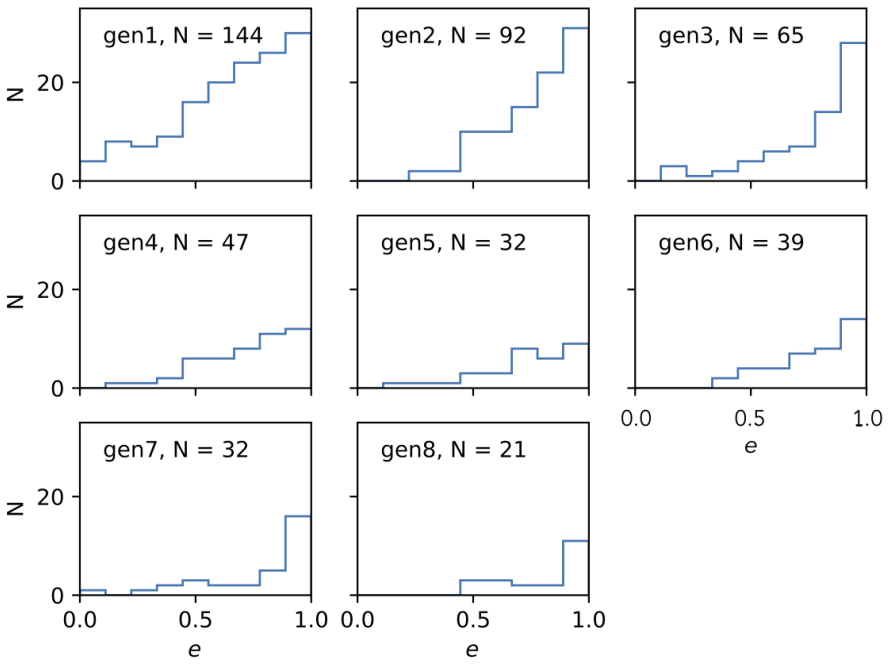

Figure 4.7: Number of ionized systems as a function of the eccentricity throughout the 8 generation for the unequal mass case.

of the mass of the binary in the bottom panel. The top panel shows how binaries with large semi-major axis form and survive if the associated eccentricity is also large. The bottom panel shows a tendency for heavier binaries to from. This can be explained since ionization is more likely for lighter systems and also exchanges favour the formation of heavier binaries [26].

I investigated whether ionization could be held responsible for the drift in eccentricity or not. This would be the case if systems with low eccentricity have a higher chance of being ionized, or if high eccentricity systems do not get ionized. In our simulations this did not seem to be the case. Fig. 4.7 shows the number of ionized binary systems as a function of the eccentricity per generation prior to the disruption for the unequal mass case. Systems with high eccentricity do indeed get ionized. The ionization process does seem to be independent on the eccentricity, and the same result is found also in [23, 16].

I investigated the relation between the change in eccentricity and the minimum distance between the intruder and the binary during the encounter in fig. 4.9. The minimum distance is computed as the smaller distance between the intruder and the component of the binary the intruder gets closest to. For both the equal and unequal mass cases I considered the variation in eccentricity due to the first set of scattering events. In the equal mass case it seems that very close encounters are associated with a $\delta e > 0$, while in the unequal mass case the trend is not as clear.

Fig. 4.10 shows the distribution of the eccentricity variation per encounter, distinguishing the encounters where an exchange takes place from those were the

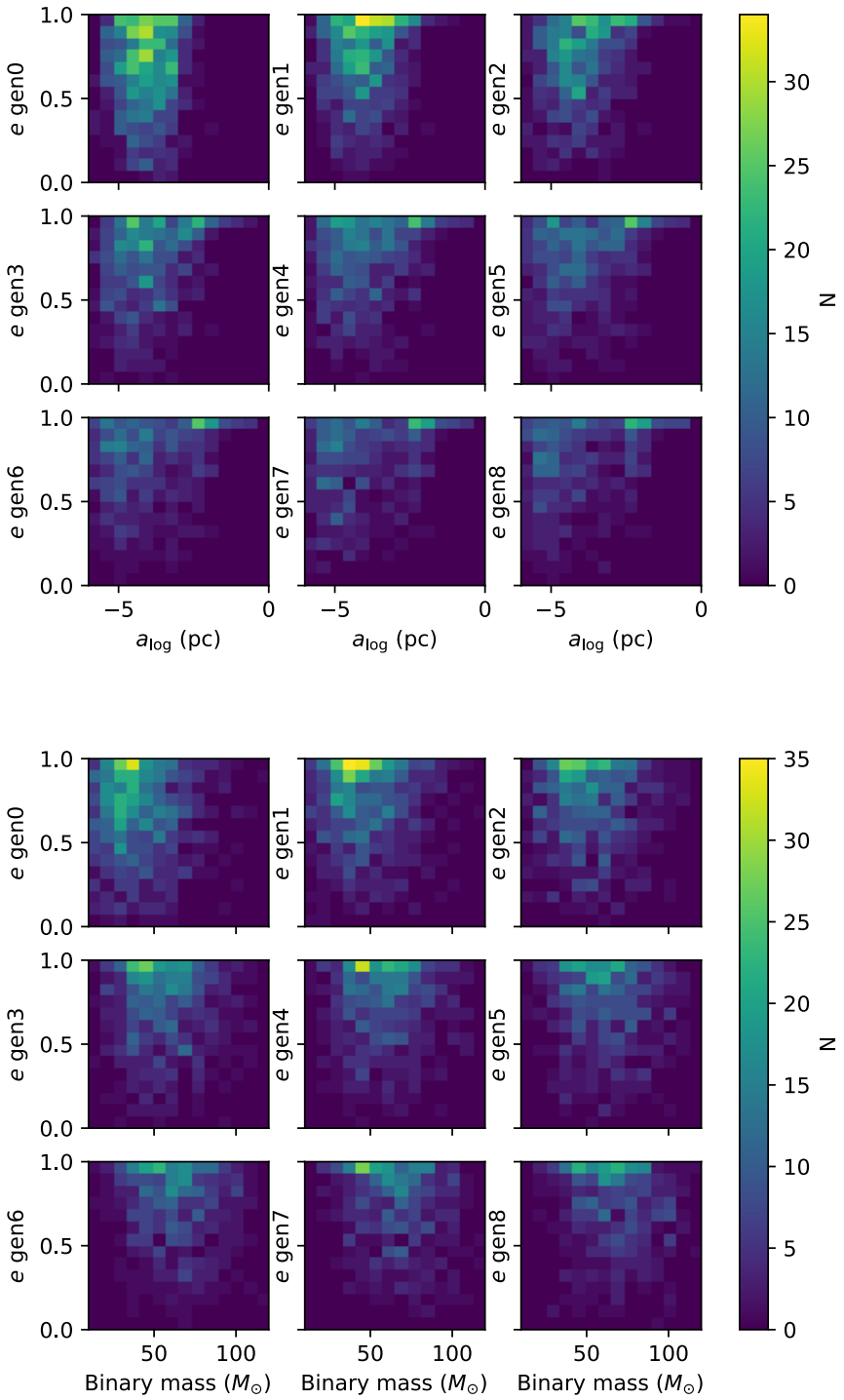

Figure 4.8: Two dimensional histograms showing the eccentricity distribution as a function of the semi-major axis distribution of the binary for different generations (top panel), and the eccentricity distribution as a function of the mass distribution for different generations (bottom panel).

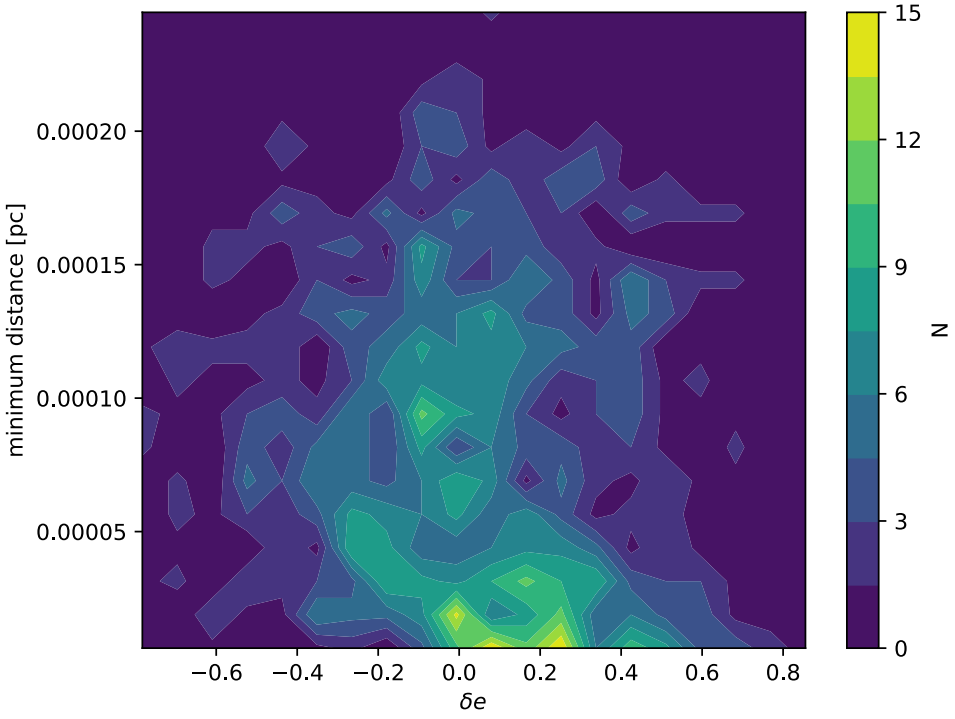

(a) Equal mass case

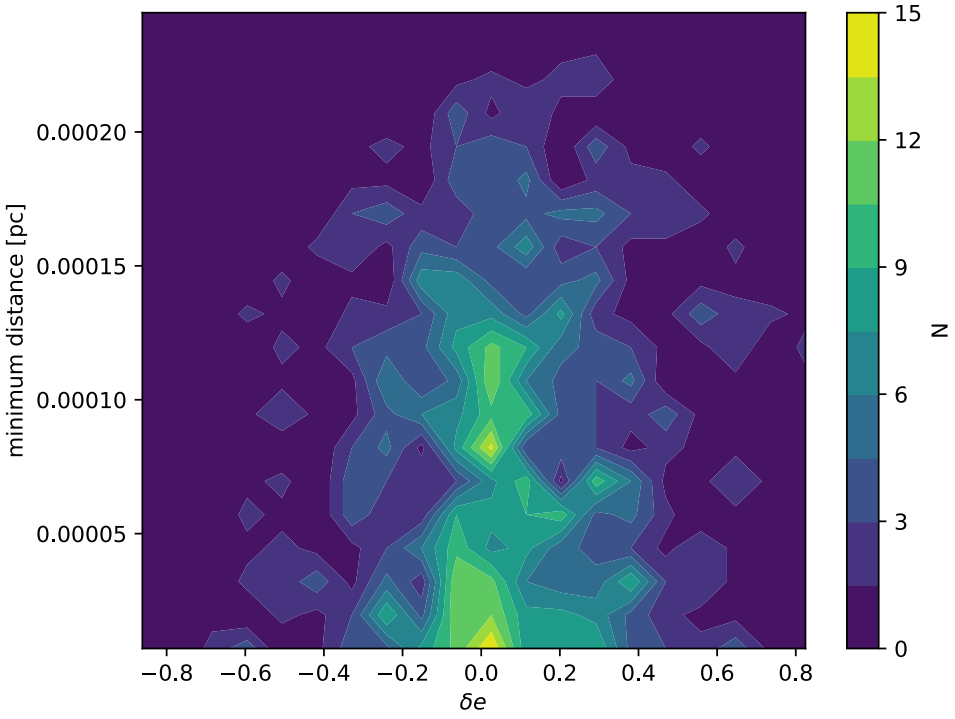

(b) Unequal mass case

Figure 4.9: Contour plots showing the relation between the minimum distance between the intruder and the components of the binary during the scattering process and the variation in eccentricity.

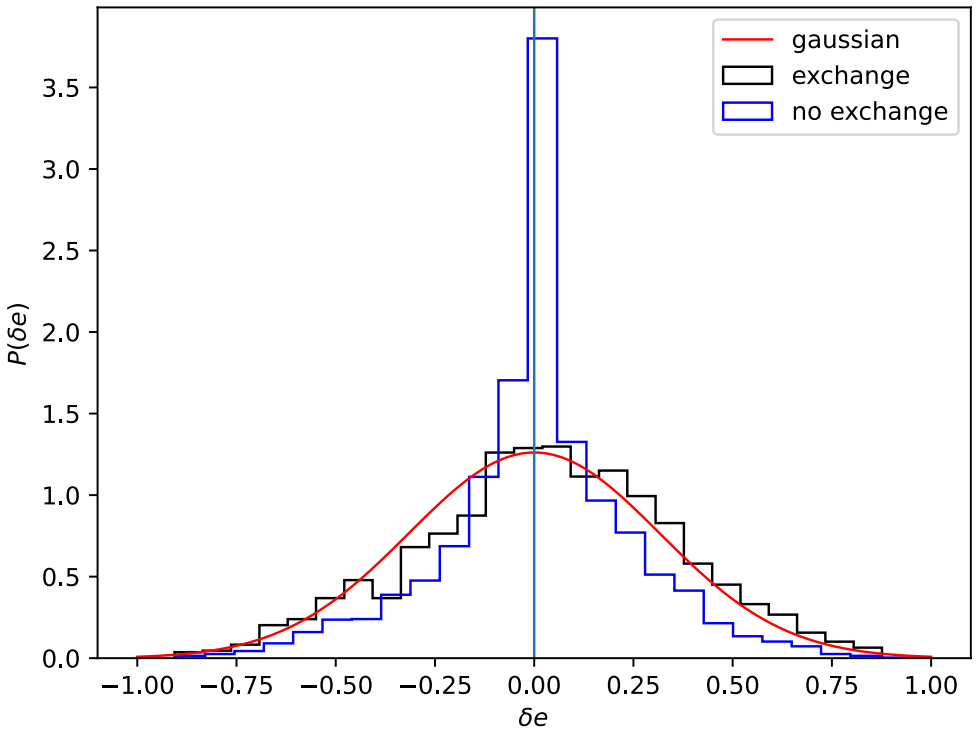

Figure 4.10: Distributions for the eccentricity variation per encounter in the unequal mass case distinguishing encounters that lead to exchanges and encounters that don't (flybys). A vertical line at $x = 0$ and a Gaussian centred in $x = 0$ are superimposed to highlight the asymmetry of the distributions.

binary components are preserved (flyby interactions), for the unequal mass case. I superimposed a Gaussian which, being symmetric by definition, highlights any asymmetries of the distributions. I was able to show that exchanges give a stronger contribution to the eccentricity change with respect to flybys, both for negative and positive changes. The strong central peak in the distribution related to flyby interactions shows how this type of interaction often does not affect the eccentricity of the binary dramatically. The Gaussian curve highlights the asymmetry of the distribution towards positive eccentricity changes, and this feature is particularly relevant for exchanges.

Chapter 5

RESULTS: Modelling equal mass binary-single encounters and the subsequent energy and eccentricity evolution of the BBHs with a Monte Carlo code

The goal of this part of my thesis is to understand the relative importance of flyby and resonant interactions with respect to the change in eccentricity that results from scattering events between a binary and an intruder. In particular I want to show how flybys play a minor role in the eccentricity change, as was also highlighted from the scattering experiments of the previous chapter. I achieved this result by means of a code that uses a Monte Carlo approach to model the energy and eccentricity evolution of a set of binaries that undergo several three-body encounter events. I chose this approach to provide a theoretical justification to this result, and also to provide an insight on the hypothesis that lead to it.

I developed a code to model the dynamical evolution of binary systems in equal mass three-body encounters, in particular focusing on the energy and eccentricity evolution of the binaries. I modeled the evolution of 10^4 equal mass binaries for a total time such that the number of scattering events per binary is ~ 100. This code adopts a Monte Carlo approach inspired by [19] and evolves the systems using analytic cross sections for the energy and eccentricity change. In my model, I considered two types of interaction: flybys and resonant interactions. I also allow for the systems to be ionized. For each type of interaction (flyby or resonant) I adopted a different prescription for the evolution of the energy and the eccentricity. I treat the energy and the eccentricity evolution as two independent processes.

Here I give an overview of how the code works, more details are provided in section 5.3. First an array of initial binaries is generated. These share some properties, i.e. the same component masses ($m_1 = m_2 = m$) and the same semi-major axis a, while each initial eccentricity is sampled from a thermal distribution. The

semi-major axis a is chosen such that the binaries are at the hard-soft boundary:

$$a = \frac{Gm}{2\sigma^2}, \tag{5.1}$$

where σ is the three-dimensional velocity dispersion of stars in the star cluster. Each binary is evolved by simulating a series of scattering events with an intruder of mass $m_3 = m$. For each encounter I sample a time between two subsequent interactions, a velocity v_3 for the intruder, I determine whether the interaction is a resonant interaction or a flyby, I sample accordingly an energy change and an eccentricity change, I determine whether the binary is ionized or not. In the following sections, I provide more details about how I implemented these processes.

5.1 Treatment of the energy evolution

The rate of a given process is described by a differential cross section. In general we define the binding energy of the binary as:

$$x = \frac{Gm_1m_2}{2a}. \tag{5.2}$$

We also define y as the amount of energy the intruder gains after the encounter, evaluated at infinity, and $\Delta = y/x$ is the fractional energy change for the binary.

We define the reaction rate function $Q(x, \Delta)$ which describes the rate of processes responsible for a fractional energy change of the binding energy of the binary by an amount between Δ and $\Delta + d\Delta$ as [43]:

$$Q(x, \Delta) \equiv \int_0^\infty VF(V)\frac{d\sigma}{d\Delta}(x, \Delta, V)d^3V, \tag{5.3}$$

where $d\sigma/d\Delta$ is the differential cross section for a fractional energy change between Δ and $\Delta + d\Delta$ and $F(V)$ is the distribution of relative velocities. We chose a Maxwellian distribution given by:

$$f(V) = \left(3\pi\sigma_V^2\right)^{-3/2} \exp\left[\frac{-V^2}{3\sigma_V^2}\right], \tag{5.4}$$

where σ_V is the velocity dispersion of single stars in the cluster, such that $\sigma = \sigma_V\sqrt{3/2}$. The average change in binding energy with time (heating rate), is computed as:

$$\langle \dot{x} \rangle = \left\langle \frac{dx}{dt} \right\rangle = n \int_{-x}^{\infty} yQ(x, \Delta)d\Delta, \tag{5.5}$$

where n is the number density of single stars in the cluster. We will neglect the interval $[-x, 0]$, performing the previous integral in the range $[0, \infty]$, to compute the heating rate shown in eq. (5.5). This is possible since in our model binaries harden at a constant rate (on average), and for hard binaries the contribution for

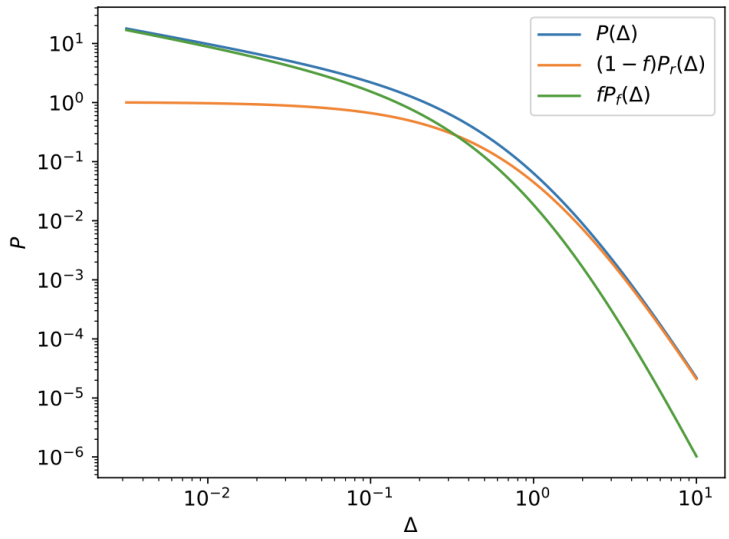

Figure 5.1: PDFs for the fractional energy change in the binding energy of the binary as a consequence of a scattering event. $P_r(\Delta)$ refers to resonant interactions (eq.(5.10)), $P_f(\Delta)$ refers to flyby interactions (eq. (5.12)), while $P(\Delta)$ refers to the combined processes (eq. (5.9)).

negative values of Δ is negligible [43].

5.1.1 Probability distribution functions (PDFs) for the energy exchange

Since we want to treat differently flybys and resonant interactions we need two different prescriptions for the fractional energy change for the two processes. Spitzer [43] provides a differential cross section for the combined processes:

$$\frac{d\sigma}{d\Delta} = \pi a^2 \frac{2AV_c^2}{\sqrt{3\pi}V^2} \frac{1}{\Delta^{1/2}(1+\Delta)^4}, \tag{5.6}$$

where $V_c = 3x/m$ for the equal mass case is the critical velocity of the intruder below which it could not disrupt the binary and A is a coefficient determined from numerical experiments. Plugging eq. (5.6) in eq. (5.5) and setting $A = 21$ [43] we get the following heating rate:

$$\dot{x} = \frac{\pi A}{16} n \frac{G^2 m^3}{\sigma_V} \simeq 4.12 n \frac{G^2 m^3}{\sigma_V}. \tag{5.7}$$

A slightly different numerical coefficient of 3.8 instead of 4.12 is reported in [17]. The heating rate in eq. (5.7) is what we ultimately want to reproduce with our code.

Combining equation 5.2 with equation 5.7 we obtain an equation that describes

the evolution of the semi-major axis (hardening) of the binaries:

$$\frac{d}{dt}\left(\frac{1}{a}\right) = \frac{2\pi A}{16}\frac{\rho G}{\sigma_V}, \tag{5.8}$$

where ρ is the local mass density of stars.

From eq. (5.6) we can get a normalized PDF for the fractional energy change for the combined processes of flyby and resonance:

$$P(\Delta) = \frac{16}{5\pi}\Delta^{-1/2}(1+\Delta)^{-4}. \tag{5.9}$$

Spitzer [43] provides also the normalized PDF for the fractional energy change for resonant processes:

$$P_r(\Delta) = (7/2)(1+\Delta)^{-9/2}. \tag{5.10}$$

Defining f as the fraction of flyby interactions and demanding that $(1-f)P_r$ converges to eq. (5.9) for large Δ we find that:

$$f = 1 - \frac{32}{35\pi} \simeq 0.7, \tag{5.11}$$

and this fraction allows us to compute the functional form of the PDF for the fractional energy change for a flyby interaction by satisfying the following condition:

$$P_f(\Delta) = f^{-1}P(\Delta) + \frac{f-1}{f}P_r(\Delta) = \\ = \frac{112}{35\pi - 32}\left(\Delta^{-1/2} - (1+\Delta)^{-1/2}\right)(1+\Delta)^{-4}. \tag{5.12}$$

The three analytic PDFs are shown in fig. 5.1.

The average fractional change in binding energy for the combined processes can be computed from eq. (5.9) as:

$$\langle\Delta\rangle = \int_0^\infty \Delta P(\Delta) d\Delta = 0.2, \tag{5.13}$$

while the average fractional changes in binding energy for flybys and resonant processes can be computed from eq. (5.10) and eq. (5.12) as:

$$\langle\Delta_f\rangle = \int_0^\infty \Delta P_f(\Delta) d\Delta \simeq 0.12, \qquad \langle\Delta_r\rangle = \int_0^\infty \Delta P_r(\Delta) d\Delta = 0.4. \tag{5.14}$$

Combining eq. (5.5) with eq. (5.9) we computed the average rate of encounters for the combined flyby and resonant processes:

$$\mathcal{R} = \frac{\dot{x}}{\langle\Delta\rangle x} \simeq 41.2an\frac{Gm}{\sigma_V}, \tag{5.15}$$

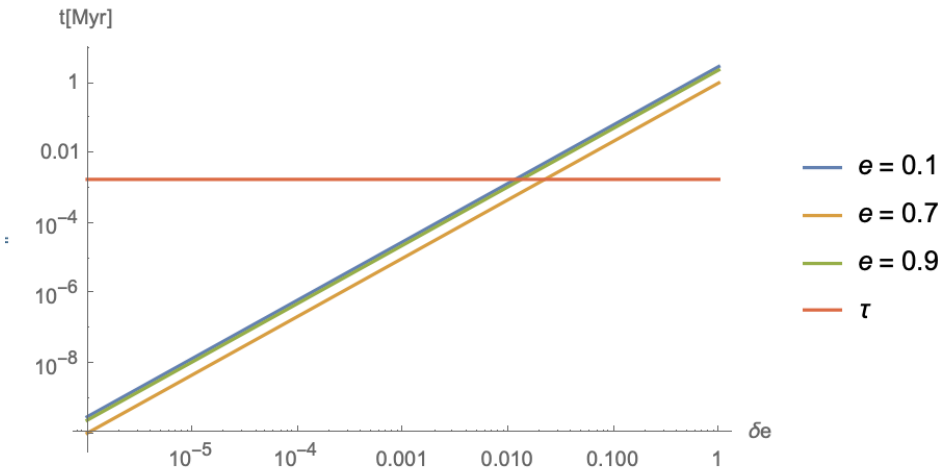

Figure 5.2: Timescales for energy and eccentricity change for different values of the eccentricity of the binary.

and the average time between interactions can therefore be computed as:

$$\tau = \mathcal{R}^{-1}. \tag{5.16}$$

It depends on cluster properties and the semi-major axis a (energy) of the binary.

5.2 Treatment of the eccentricity evolution

Our code evolves the eccentricity of each binary in two different ways depending on whether the interaction is resonant or a flyby. For the flyby case we considered the following cross section from [18]:

$$\sigma\left(\delta e > \delta e_0\right) = \frac{9}{14\pi}\frac{3^{1/2}}{6^{1/3}}\left(\frac{15\pi}{4}\right)^{2/3}\left[\Gamma\left(\frac{2}{3}\right)\Gamma\left(\frac{5}{6}\right)\right]^2\frac{3Gma}{V^2}e^{2/3}\left(1-e^2\right)^{1/3}\delta e_0^{-2/3}, \tag{5.17}$$

valid in this shape for the equal mass case. This cross section describes changes in eccentricity that satisfy $\delta e > \delta e_0$. In order to obtain the rate of processes that change the eccentricity according to this formula we computed the following differential cross section by taking the derivative with respect to δe_0 of (5.17):

$$\frac{d\sigma}{d\delta e_0} = \frac{3}{7\pi}\frac{3^{1/2}}{6^{1/3}}\left(\frac{15\pi}{4}\right)^{2/3}\left[\Gamma\left(\frac{2}{3}\right)\Gamma\left(\frac{5}{6}\right)\right]^2\frac{3Gma}{V^2}e^{2/3}\left(1-e^2\right)^{1/3}\delta e_0^{-5/3}, \tag{5.18}$$

disregarding the minus sign. We than computed the interaction time scale as:

$$\tau_e = \left(n\frac{d\sigma}{d\delta e_0}v\right)^{-1}. \tag{5.19}$$

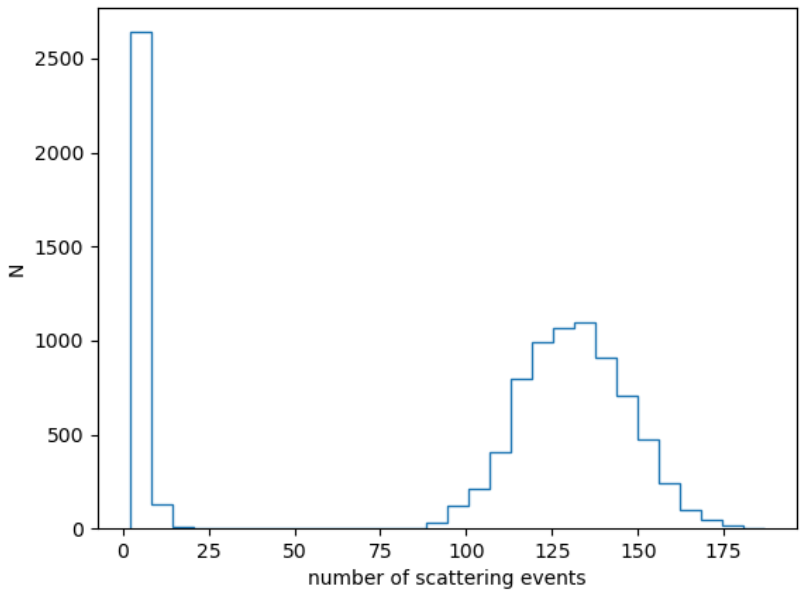

Figure 5.3: The number of systems as a function of the number of scattering events they undergo. The peak is due to the fact that binaries tend to get ionized in the first encounters, when the have not hardened enough and intruders carry enough energy to disrupt them.

In fig. 5.19 we compared the timescales for energy change (eq. (5.16)) and eccentricity change (eq. (5.19)) for different values of the eccentricity of the binary considering the properties of a globular cluster. This showed us that we can expect, in our model, that a flyby interaction contributes to the eccentricity change by roughly 1%. Therefore as the PDF for eccentricity change we considered the following power law from eq. (5.18):

$$P_f(e) \propto \delta e_0^{-5/3}, \tag{5.20}$$

normalized in the range $[10^{-6}, 10]$. Small variations of the eccentricity are far more likely, but we allow for $\delta e > 1$ in consideration of hyperbolic orbits.

The prescription we chose for the eccentricity evolution due to resonant encounters arises from the consideration that such encounters are chaotic processes. Resonant encounters quickly loose memory of their initial conditions [41]. The outcome of a chaotic process will depend on an underlying probability distribution which for the purpose of this code we chose as thermal.

5.3 The code

As we mentioned the code starts by generating an array of binary systems with mass m and semi-major axis a at the hard-soft boundary. The initial eccentricity

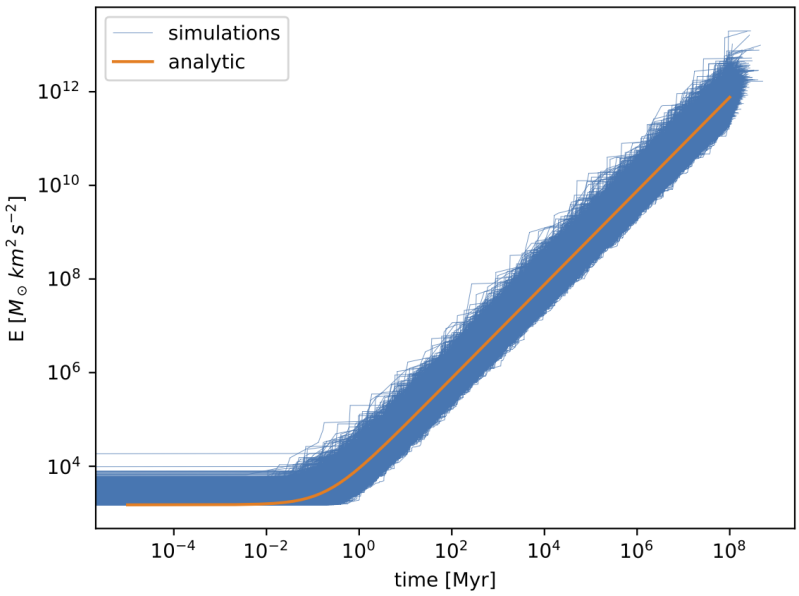

Figure 5.4: Here we show the binding energy evolution with time, for all the binaries in the simulation, as a consequence of the hardening process induced by three-body interactions. The heating rate matches the analytic prediction of eq. (5.7).

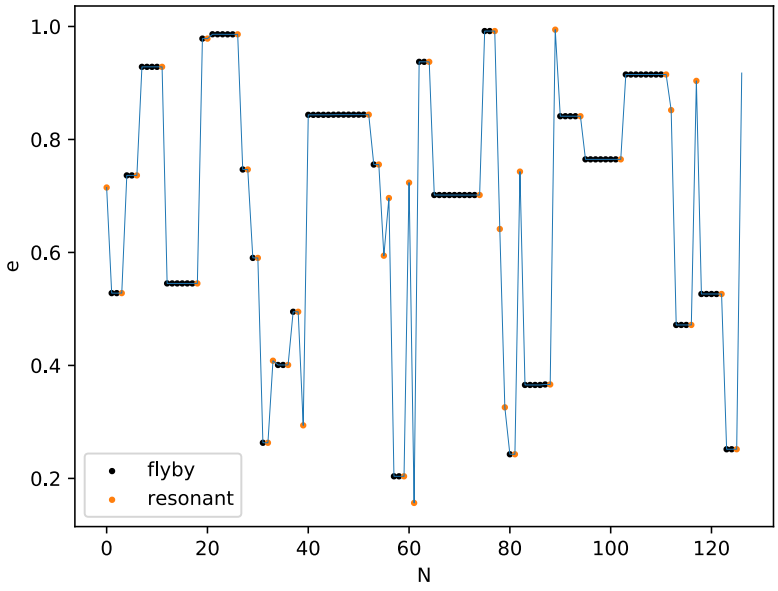

Figure 5.5: Eccentricity evolution of a binary after $\sim$ 120 three-body scattering events

of the binaries is sampled from a thermal distribution. Then an array of intruders is generated, again with mass m and incoming velocity sampled from a Maxwellian (eq. (5.4)). In order to sample from this distribution we take advantage of the fact that it cam be randomly sampled as $v = \sqrt{x^2 + y^2 + z^2}$, where x, y and z are three Gaussian random numbers, with a probability distribution function centered in zero and with the same σ as the Maxwellian. At this point the encounters are performed.

For each binary and each encounter the code samples an interaction time from eq. (5.16) with the exponential law:

$$P(t_{int}) = 1 - \exp^{-t_{int}/\tau}, \tag{5.21}$$

and therefore:

$$t_{int} = -\tau \log(1 - R), \tag{5.22}$$

where R is a uniform random number in the range [0,1].

The code then determines, for each encounter, the nature of the process, i.e. whether it is a flyby or a resonant encounter. This is randomly determined using the fraction computed in eq. (5.11).

For each encounter the energy end eccentricity are evolved according to the type of interaction. For the eccentricity change due to flybys the code also randomly samples a sign to determine whether the eccentricity change from eq. (5.20) will be positive or negative. Equal probability is assigned to the two options, following [18].

We also determine if a given encounter ionizes a systems with the following prescription: the system is ionized with a probability of 50% if the velocity of the intruder is in the interval $[1.2V_c, 10V_c]$ [22]. $V_c = 3x/m$ is the critical velocity to disrupt the binary. The upper limit can be understood also intuitively since very fast encounters do not have time to exchange enough energy. We also assume that the ionization process is independent of the eccentricity of the binary [23, 16]. The number of systems as a function of the number of scattering events they undergo is shown in fig. 5.3. The figure shows how ionization takes place during the first scattering events (as shown by the peak of systems that undergo only few encounters), when $\sim$ 28% of the binaries are ionized. After the first encounters binaries start to get too hard for the single stars to have enough energy to allow for ionizations to take place. The number of scattering events for binaries that are not ionized during the first encounters is spread around $\sim$ 130 since we simulate each binary for the same total time.

With these prescriptions the code is able to reproduce the heating rate $\dot{x}$ of eq. (5.7). This can be seen from fig. 5.4, which shows the evolution of the binding energy of each binary system caused by scattering events with single stars, together with the analytic heating rate of eq. (5.7). Fig. 5.5 instead shows the eccentricity evolution for a random system simulated with this code. We can see how flyby interactions, contribute very little to eccentricity evolution of the system. This can also be seen from figure 5.6, where we compare the distributions of the variation of eccentricity per encounter for the two processes. Flyby contributions are all

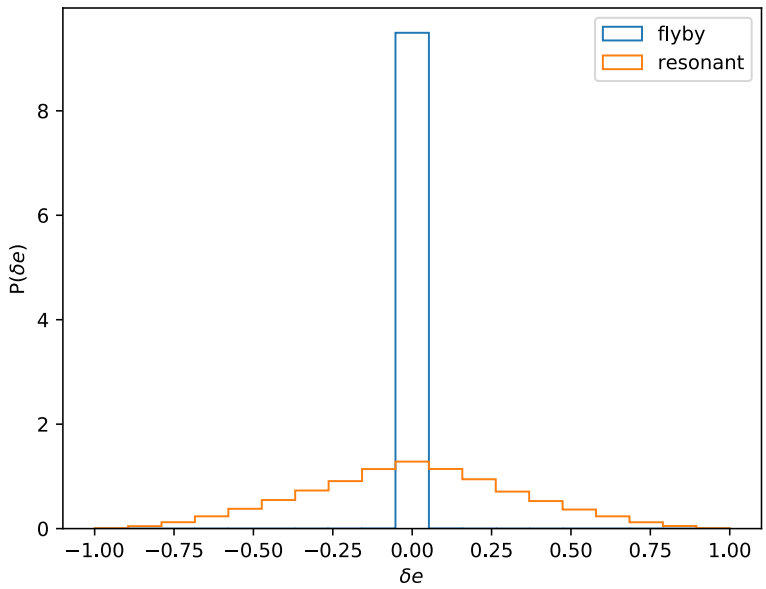

Figure 5.6: Distributions of the eccentricity variation for flyby and resonant interactions. All flyby contributions are concentrated in a central bin, with more than 90% of $|\delta e|$ below 10^{-4}.

concentrated in the central bin, with over 90% of $|\delta e|$ below 10^{-4}. This result agrees with what we found in the previous chapter, namely that flyby interactions play a marginal role in the eccentricity evolution of hard binaries as a consequence of scattering events. Fig. 5.6 and fig. 4.10 do share some features, such as the peaked distribution for flyby interactions and the gaussian-like distribution for resonant encounters. However, the prescription we chose is not able to describe the full shape of the eccentricity variation distribution for flyby interactions we found with the N-body simulations.

Chapter 6

Conclusions and further developments

In this thesis I presented the theoretical background needed for the description of three body encounters between a hard binary and an intruder, in order to perform numerical experiments to determine the eccentricity evolution induced by the scattering events on such binaries. I simulated two sets of 10^3 individual binary-single encounters with the high precision N-body code ARWV [7], for equal and unequal mass binaries. I demonstrated that the encounters increase the average eccentricity of the binaries, initially distributed following a thermal eccentricity distribution. In particular I found that the fraction of systems with eccentricity $e > 0.9$ increases on average by $\sim 15\%$ after each encounter for the equal mass case and by $\sim 7.7\%$ in the unequal mass case. I also ran smaller scale simulations with different initial distributions for the eccentricities, finding that this effect is present also when starting with a uniform eccentricity distribution and with a low-eccentricity distribution. I demonstrated that this effect is not due to the disruption via ionization of low-eccentricity binaries, confirming that the ionization probability is essentially independent of eccentricity. I showed that the mass of the binaries tends to increase as a consequence of exchanges. I investigated the relation between the increase in eccentricity and the minimum distance of the encounter, finding a mild tendency for very close encounters to increase the eccentricity, stronger in the equal mass case. I demonstrated that exchanges have a stronger effect on eccentricity changes compared to flybys both via the N-body scattering experiments and via the development of a Monte Carlo code able to simulate the energy and eccentricity evolution of equal mass binaries undergoing binary single encounters. This code is much faster compared to the N-body experiments, but is limited by some simplifying assumptions.

For what concerns further developments, an interesting one is that the results I obtained can be used to determine fitting formulae to be used by semi-analytic codes to model the eccentricity evolution of hard binaries. One example of these codes is FASTCLUSTER [27], which is able to simulate hierarchical BBH mergers at a low computational cost. Computational cost is one of the main challenges in modelling hierarchical mergers, and semi-analytic codes allow to probe a large parameter

otherwise impossible with N-body codes. Moreover, different prescriptions for the eccentricity evolution could have an impact on the merger rate of BBHs.

Bibliography

[1] B. P. Abbott et al. Observation of Gravitational Waves from a Binary Black Hole Merger. , 116(6):061102, Feb. 2016. doi:10.1103/PhysRevLett.116.061102.

[2] P. Amaro-Seoane et al. Laser Interferometer Space Antenna. *arXiv e-prints*, art. arXiv:1702.00786, Feb. 2017.

[3] A. Askar, M. Szkudlarek, D. Gondek-Rosińska, M. Giersz, and T. Bulik. MOCCA-SURVEY Database - I. Coalescing binary black holes originating from globular clusters. , 464(1):L36–L40, Jan. 2017. doi:10.1093/mnrasl/slw177.

[4] M. J. Benacquista and J. M. B. Downing. Relativistic Binaries in Globular Clusters. *Living Reviews in Relativity*, 16(1):4, Mar. 2013. doi:10.12942/lrr-2013-4.

[5] S. Chandrasekhar. Dynamical Friction. I. General Considerations: the Coefficient of Dynamical Friction. , 97:255, Mar. 1943. doi:10.1086/144517.

[6] P. Chassonnery and R. Capuzzo-Dolcetta. Dynamics of a superdense cluster of black holes and the formation of the Galactic supermassive black hole. , 504 (3):3909–3921, June 2021. doi:10.1093/mnras/stab1016.

[7] P. Chassonnery, R. Capuzzo-Dolcetta, and S. Mikkola. ARWV Code User Manual. *arXiv e-prints*, art. arXiv:1910.05202, Oct. 2019.

[8] M. Dall'Amico, M. Mapelli, U. N. Di Carlo, Y. Bouffanais, S. Rastello, F. Santoliquido, A. Ballone, and M. Arca Sedda. GW190521 formation via three-body encounters in young massive star clusters. , 508(2):3045–3054, Dec. 2021. doi:10.1093/mnras/stab2783.

[9] U. N. Di Carlo, M. Mapelli, Y. Bouffanais, N. Giacobbo, F. Santoliquido, A. Bressan, M. Spera, and F. Haardt. Binary black holes in the pair instability mass gap. , 497(1):1043–1049, Sept. 2020. doi:10.1093/mnras/staa1997.

[10] R. Elson, P. Hut, and S. Inagaki. Dynamical evolution of globular clusters. , 25:565–601, Jan. 1987. doi:10.1146/annurev.aa.25.090187.003025.

[11] A. M. Geller, N. W. C. Leigh, M. Giersz, K. Kremer, and F. A. Rasio. In Search of the Thermal Eccentricity Distribution. , 872(2):165, Feb. 2019. doi:10.3847/1538-4357/ab0214.

[12] N. Giacobbo and M. Mapelli. The progenitors of compact-object binaries: impact of metallicity, common envelope and natal kicks. , 480(2):2011–2030, Oct. 2018. doi:10.1093/mnras/sty1999.

[13] N. Giacobbo, M. Mapelli, and M. Spera. Merging black hole binaries: the effects of progenitor's metallicity, mass-loss rate and Eddington factor. , 474 (3):2959–2974, Mar. 2018. doi:10.1093/mnras/stx2933.

[14] Y. B. Ginat and H. Perets. Analytic Modelling of Binary-Single Encounters: Non-Thermal Eccentricity Distribution and Gravitational-Wave Source Formation. *arXiv e-prints*, art. arXiv:2205.15957, May 2022.

[15] R. Gratton, A. Bragaglia, E. Carretta, V. D'Orazi, S. Lucatello, and A. Sollima. What is a globular cluster? An observational perspective. , 27(1):8, Nov. 2019. doi:10.1007/s00159-019-0119-3.

[16] D. C. Heggie. Binary evolution in stellar dynamics. , 173:729–787, Dec. 1975. doi:10.1093/mnras/173.3.729.

[17] D. C. Heggie and P. Hut. Binary–Single-Star Scattering. IV. Analytic Approximations and Fitting Formulae for Cross Sections and Reaction Rates. , 85: 347, Apr. 1993. doi:10.1086/191768.

[18] D. C. Heggie and F. A. Rasio. The Effect of Encounters on the Eccentricity of Binaries in Clusters. , 282(3):1064–1084, Oct. 1996. doi:10.1093/mnras/282.3.1064.

[19] D. C. Heggie, S. Portegies Zwart, and J. R. Hurley. McScatter: A simple three-body scattering package with stellar evolution. , 12(1):20–28, Oct. 2006. doi:10.1016/j.newast.2006.04.005.

[20] M. Henon. Vlasov equation. , 114(1):211, Oct. 1982.

[21] J. G. Hills and L. W. Fullerton. Computer simulations of close encounters between single stars and hard binaries. , 85:1281–1291, Sept. 1980. doi:10.1086/112798.

[22] P. Hut. Binaries as a heat source in stellar dynamics - Release of binding energy. , 272:L29–L33, Sept. 1983. doi:10.1086/184111.

[23] P. Hut and J. N. Bahcall. Binary-single star scattering. I - Numerical experiments for equal masses. , 268:319–341, May 1983. doi:10.1086/160956.

[24] J. H. Jeans. The origin of binary systems. , 79:408, Apr. 1919. doi:10.1093/mnras/79.6.408.

[25] P. Kroupa. Initial Conditions for Star Clusters. In S. J. Aarseth, C. A. Tout, and R. A. Mardling, editors, *The Cambridge N-Body Lectures*, volume 760, page 181. 2008. doi:10.1007/978-1-4020-8431-7_8.

[26] M. Mapelli. Formation Channels of Single and Binary Stellar-Mass Black Holes. In *Handbook of Gravitational Wave Astronomy*, page 16. 2021. doi:10.1007/978-981-15-4702-7_16-1.

[27] M. Mapelli, M. Dall'Amico, Y. Bouffanais, N. Giacobbo, M. Arca Sedda, M. C. Artale, A. Ballone, U. N. Di Carlo, G. Iorio, F. Santoliquido, and S. Torniamenti. Hierarchical black hole mergers in young, globular and nuclear star clusters: the effect of metallicity, spin and cluster properties. , 505(1):339–358, July 2021. doi:10.1093/mnras/stab1334.

[28] M. Mapelli, M. Dall'Amico, Y. Bouffanais, N. Giacobbo, M. Arca Sedda, M. C. Artale, A. Ballone, U. N. Di Carlo, G. Iorio, F. Santoliquido, and S. Torniamenti. Hierarchical black hole mergers in young, globular and nuclear star clusters: the effect of metallicity, spin and cluster properties. , 505(1):339–358, July 2021. doi:10.1093/mnras/stab1334.

[29] S. Mikkola and D. Merritt. Implementing Few-Body Algorithmic Regularization with Post-Newtonian Terms. , 135(6):2398–2405, June 2008. doi:10.1088/0004-6256/135/6/2398.

[30] S. Mikkola and K. Tanikawa. Algorithmic regularization of the few-body problem. , 310(3):745–749, Dec. 1999. doi:10.1046/j.1365-8711.1999.02982.x.

[31] S. Mikkola and K. Tanikawa. Explicit Symplectic Algorithms For Time-Transformed Hamiltonians. *Celestial Mechanics and Dynamical Astronomy*, 74(4):287–295, Aug. 1999. doi:10.1023/A:1008368322547.

[32] A. P. Milone, A. F. Marino, L. R. Bedin, A. Dotter, H. Jerjen, D. Kim, D. Nardiello, G. Piotto, and J. Cong. The binary populations of eight globular clusters in the outer halo of the Milky Way. , 455(3):3009–3019, Jan. 2016. doi:10.1093/mnras/stv2415.

[33] P. C. Peters. Gravitational Radiation and the Motion of Two Point Masses. *Physical Review*, 136(4B):1224–1232, Nov. 1964. doi:10.1103/PhysRev.136.B1224.

[34] H. C. Plummer. The distribution of stars in globular clusters. , 76:107–121, Dec. 1915. doi:10.1093/mnras/76.2.107.

[35] S. F. Portegies Zwart and S. L. W. McMillan. Black Hole Mergers in the Universe. , 528(1):L17–L20, Jan. 2000. doi:10.1086/312422.

[36] S. F. Portegies Zwart, S. L. W. McMillan, and M. Gieles. Young Massive Star Clusters. , 48:431–493, Sept. 2010. doi:10.1146/annurev-astro-081309-130834.

[37] C. L. Rodriguez, S. Chatterjee, and F. A. Rasio. Binary black hole mergers from globular clusters: Masses, merger rates, and the impact of stellar evolution. , 93(8):084029, Apr. 2016. doi:10.1103/PhysRevD.93.084029.

[38] J. Samsing and D. J. D'Orazio. Black Hole Mergers From Globular Clusters Observable by LISA I: Eccentric Sources Originating From Relativistic N-body Dynamics. , 481(4):5445–5450, Dec. 2018. doi:10.1093/mnras/sty2334.

[39] H. Sana, S. E. de Mink, A. de Koter, N. Langer, C. J. Evans, M. Gieles, E. Gosset, R. G. Izzard, J. B. Le Bouquin, and F. R. N. Schneider. Binary Interaction Dominates the Evolution of Massive Stars. *Science*, 337(6093):444, July 2012. doi:10.1126/science.1223344.

[40] S. Sigurdsson and L. Hernquist. Primordial black holes in globular clusters. , 364(6436):423–425, July 1993. doi:10.1038/364423a0.

[41] S. Sigurdsson and E. S. Phinney. Binary–Single Star Interactions in Globular Clusters. , 415:631, Oct. 1993. doi:10.1086/173190.

[42] J. Spitzer, Lyman and M. H. Hart. Random Gravitational Encounters and the Evolution of Spherical Systems. I. Method. , 164:399, Mar. 1971. doi:10.1086/150855.

[43] L. Spitzer. *Dynamical evolution of globular clusters*. 1987.